Gas Seepage and Pockmark Formation From Subsurface Reservoirs: Insights From Table-Top Experiments

Vaknin, I., Aharonov, E., Holtzman, R. & Katz, O.

DOI 10.1029/2023JB028255
ISSN 2169-9313
ESSN 2169-9356

Publisher: Wiley

JGR Solid Earth

RESEARCH ARTICLE
10.1029/2023JB028255

Gas Seepage and Pockmark Formation From Subsurface Reservoirs: Insights From Table-Top Experiments

I. Vaknin[1], E. Aharonov[1], R. Holtzman[2], and O. Katz[3]

[1]Institute of Earth Sciences, The Hebrew University of Jerusalem, Jerusalem, Israel, [2]Centre for Fluid and Complex Systems, Coventry University, Coventry, UK, [3]Geological Survey of Israel, Jerusalem, Israel

Key Points:

- Sandbox experiments link pockmark morphology (irregular vs. conical) to gas seepage-induced deformation of the host (seal) layer
- Experiments and theory show seal thickness and consolidation control deformation mechanism: doming, brittle (faults), or plastic (bubbles)
- Theoretical calculations predict that under field conditions, the preferred mechanism for gas escape will be bubbles rising in faults

Supporting Information:

Supporting Information may be found in the online version of this article.

Correspondence to:

E. Aharonov and R. Holtzman,
einatah@mail.huji.ac.il;
ran.holtzman@coventry.ac.uk

Citation:

Vaknin, I., Aharonov, E., Holtzman, R., & Katz, O. (2024). Gas seepage and pockmark formation from subsurface reservoirs: Insights from table-top experiments. *Journal of Geophysical Research: Solid Earth*, *129*, e2023JB028255. https://doi.org/10.1029/2023JB028255

Received 20 NOV 2023
Accepted 21 MAR 2024

Author Contributions:

Conceptualization: I. Vaknin, E. Aharonov, R. Holtzman
Formal analysis: I. Vaknin, E. Aharonov, R. Holtzman, O. Katz
Funding acquisition: E. Aharonov, R. Holtzman
Investigation: I. Vaknin, E. Aharonov, R. Holtzman, O. Katz
Methodology: I. Vaknin, E. Aharonov, R. Holtzman, O. Katz
Project administration: E. Aharonov, R. Holtzman
Supervision: E. Aharonov, R. Holtzman, O. Katz

Abstract Pockmarks are morphological depressions commonly observed in ocean and lake floors. Pockmarks form by fluid (typically gas) seepage thorough a sealing sedimentary layer, deforming and breaching the layer. The seepage-induced sediment deformation mechanisms, and their links to the resulting pockmarks morphology, are not well understood. To bridge this gap, we conduct laboratory experiments in which gas seeps through a granular (sand) reservoir, overlaid by a (clay) seal, both submerged under water. We find that gas rises through the reservoir and accumulates at the seal base. Once sufficient gas over-pressure is achieved, gas deforms the seal, and finally escapes via either: (a) doming of the seal followed by dome breaching via fracturing; (b) brittle faulting, delineating a plug, which is lifted by the gas seeping through the bounding faults; or (c) plastic deformation by bubbles ascending through the seal. The preferred mechanism is found to depend on the seal thickness and stiffness: in stiff seals, a transition from doming and fracturing to brittle faulting occurs as the thickness increases, whereas bubble rise is preferred in the most compliant, thickest seals. Seepage can also occur by mixed modes, such as bubbles rising in faults. Repeated seepage events suspend the sediment at the surface and create pockmarks. We present a quantitative analysis that explains the tendency for the various modes of deformation observed experimentally. Finally, we connect simple theoretical arguments with field observations, highlighting similarities and differences that bound the applicability of laboratory experiments to natural pockmarks.

Plain Language Summary Pockmarks are pit-like depressions common in ocean and lake floors, formed by gas seepage through underlying sediments. Despite relevance to both fossil fuel exploration and global warming, the mechanisms by which pockmarks evolve remain elusive. We conduct simple laboratory experiments in which we inject air into a layer of glass beads (”reservoir”) overlain by a layer of clay (”seal”), all submerged underwater in a transparent box. We find that gas rises through the sand and accumulates at the base of the clay. Then, gas pressure rises until it suffices to deform the clay and escape, forming a pockmark. This occurs by one of three mechanisms, depending on clay thickness and stiffness: (a) heaving of a dome which then fractures in thin clay layers; (b) faulting in thick, stiff clays; and (c) bubbles ascend in thick, soft clays. Pipe-like focused gas conduits connecting the clay bottom to the pockmark are created by the rise of a “trains” of bubbles that weaken their path. These pathways can also initiate in faults. Repeated seepage events push the clay particles, suspending them in water to create a pockmark. Our findings agree with field observations, improving our understanding of natural pockmark formation.

1. Introduction

Gas seepage from oceanic and lacustrine sediments is globally prevalent, forming geological structures such as pockmarks, vents, and mud volcanoes along the continental margins at many locations (de Mahiques et al., 2017; Dupré et al., 2010; Hovland et al., 2005; King & MacLean, 1970; Krämer et al., 2017; Pilcher & Argent, 2007; Riedel et al., 2020; Schattner et al., 2012; Skarke et al., 2014; Sultan et al., 2010; Q. Sun et al., 2012). Oceanic gas seeps introduce large quantities of methane into the water body, up to ∼65 Tg/yr from continental shelves alone (Hovland et al., 1993; Skarke et al., 2014). Methane venting affects ocean acidification, de-oxygenation, and thus the global climate (Archer et al., 2009; Hornbach et al., 2004; McGinnis et al., 2006; Svensen et al., 2004). In particular, methane, a highly potent greenhouse gas, has a crucial role in the global carbon cycle and has been proposed as the cause of past episodes of climate change (e.g., Archer et al., 2009; Dickens, 2003; Westbrook et al., 2009). Furthermore, many seeps originate from oil and gas reservoirs as well as methane hydrate deposits, and thus can serve to indicate their location (Abrams, 2005). All these make understanding of gas seeps an important topic (Berndt, 2005).

Writing – original draft: I. Vaknin, E. Aharonov, R. Holtzman, O. Katz
Writing – review & editing: I. Vaknin, E. Aharonov, R. Holtzman, O. Katz

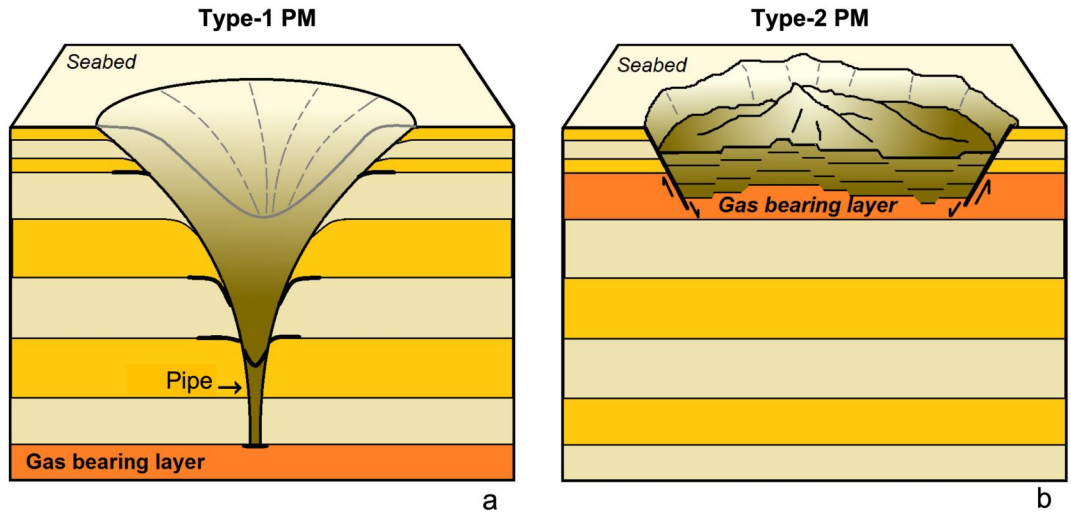

Figure 1. Geometrical characteristics of the two types of pockmarks: (a) Type-1 pockmarks are circular depression, associated with a gas pipe; (b) Type-2 pockmarks are irregular and distorted depressions. The schematic depicts only the *active* gas pipe, embedded within a much wider disturbed zone which also includes dormant pipes, reflecting the history of gas seepage.

Gas seepage from the seafloor occurs via two main mechanisms: (a) diffuse (non-focused) capillary invasion through the sediment pores (especially in coarse-grained sediments); or (b) focused preferential flow paths, along pre-existing faults and cracks or "pipes" opened by deformation induced by the fluids themselves as they migrate (Jain & Juanes, 2009; Fauria & Rempel, 2011; Holtzman et al., 2012; Z. Sun & Santamarina, 2019). The latter typically release large amounts of gas in an episodic and/or cyclic manner (Hovland et al., 2002, 2010), and are associated with pockmarks as well as vents and mud volcanoes. Pockmarks (PMs) are of particular importance due to their abundance as well as their role as markers for gas-induced sediment deformation and breaching which leads to seepage (King & MacLean, 1970; Schattner et al., 2016). Despite the importance of PMs as the surficial manifestation of the gas seepage, the mechanisms and the consequent spatiotemporal signature of the seeps remain elusive (Hovland et al., 2010). Here, we use laboratory experiments and theoretical analysis to explore the links between gas-induced sediment deformation, seepage, pockmark formation and their spatiotemporal evolution.

1.1. Field Observations of Pockmarks and Gas Pipes

Pockmarks are depressions within the surface of oceanic and lacustrine sediments, where their formation mechanism is believed to be tightly linked to the fluid seepage mechanism feeding them (King & MacLean, 1970; Schattner et al., 2016). PM diameters can range between meters and hundreds of meters. They are widespread in continental shelves (Schattner et al., 2012, 2016), slopes (Bøe et al., 1998; Gay et al., 2006; Pilcher & Argent, 2007), the deep abyss (Camerlenghi et al., 1995; A. G. Judd, 2003), deep-sea fans (Bayon et al., 2009; Loncke & Mascle, 2004), lakes, bays, estuaries (García-Gil, 2003) and fjords (Forwick et al., 2009; Hovland et al., 2002). Within seismic cross-sections, PMs are often associated with feeding pipes of incoherent signature, which suggest gas presence or liquefied or disturbed sediments (e.g., Cartwright & Santamarina, 2015).

Field observations suggest that the morphology, spatial distribution, and temporal characteristics of PMs are controlled by the geological context in which they are formed (Pilcher & Argent, 2007). Their presence and morphology are tightly linked to the fluid escape mechanisms that feed them (Cartwright et al., 2007). Pockmarks can be generally categorized according to their morphology into two types (Figure 1): (a) conical depressions termed "Type-1"; and (b) shallower, more irregular and distorted "Type-2" pockmarks (Riboulot et al., 2016). In Type-1, the sediment in the center of the structure is completely removed or in suspension, while the pockmark walls retain an angle of repose; this suggests that the sediment underwent a more granular or plastic deformation (Cathles et al., 2010). In contrast, in Type-2 pockmarks both the original strata and the disrupting faults are easily recognized, suggesting a more solid-like or brittle deformation. The significant difference in the structure of the two types suggests a different formation mechanism, such as the origin of the emitted gas: Type-1 usually

originates from deeper oil and gas reservoirs (Cathles et al., 2010), whereas Type-2 has been associated with near-surface gas hydrate layers (Riboulot et al., 2016). Although Type-2 pockmarks are found in many sites (Dillon et al., 1998; Macelloni et al., 2012; Riboulot et al., 2016; Simonetti et al., 2013; Sultan et al., 2010) they are far less common than Type-1.

1.2. Potential Formation Mechanisms of Pipes and Pockmarks

Several mechanisms have been proposed for the formation of fluid escape features and their associated pockmark structures (Cartwright & Santamarina, 2015):

1. *Hydraulic fracturing*: this mechanism assumes fluid overpressure within or under a brittle sediment layer. If the fluid pressure rises, it may fracture the overlying seal, propagating a network of hydraulic fractures toward the surface. The connected fractures form a breccia pipe. Growth in this case is suggested to culminate in explosive venting, leaving a dent at the surface (Davies et al., 2012; Løseth et al., 2011; Moss & Cartwright, 2010; Plaza-Faverola et al., 2010, 2011). We note that this mechanism of pipe formation and seepage by hydraulic fracturing is not supported by laboratory experiments.
2. *Capillary barriers forming a flat piston*: in this mechanism, proposed by Cathles et al. (2010), gas rises in a water-saturated reservoir and accumulates at its top, capped by an overlying low permeability seal. Since the seal is water-saturated and has a much smaller grain size than the underlying reservoir, the gas-water interface at the base of the seal forms a "capillary barrier" (Morel-Seytoux, 1993) which resists both the ascent of gas and the descent of water. As gas pressure rises it will plastically deform the seal, forming an upward-propagating capillary barrier that acts as a flat-roofed gas "piston." The invasion and upward propagation of the piston requires liquefaction of the sediment in front of it (Ramos et al., 2015; Varas et al., 2011). Cathles et al. (2010) estimated that once the piston ascends halfway to the surface its ascent accelerates, and once the piston gets close to the seafloor a PM of width similar to the piston forms rapidly. Although in our experiments (below) we do observe the formation of pistons at the reservoir-seal interface, they do not propagate toward the surface, as predicted by Cathles et al. (2010). (Nor are we aware of any previous experiments in which a piston ascends.)
3. *Erosive fluidization*: sediment fluidization occurs when pressure gradients exerted by pore fluids on sediment grains ("seepage forces") exceed the lithostatic stress that holds the grains in place. Seepage induced fluidization has been suggested to form PMs and mud volcanoes (Brown, 1990; Nermoen et al., 2010). Within this mechanism, one can include also the "pore-fluid escape" mechanism that occurs during compaction-induced dewatering (Böttner et al., 2019; Harrington, 1985). Cone-shaped structures, which widen toward the surface, such as the Type-1 PMs and the associated feeding pipe in Figure 1a, are often observed in the field (Riboulot et al., 2016). Similar cone-shaped structures have been shown experimentally to form under a high upwards fluid flux through submerged grain layers (Ramos et al., 2015; Varas et al., 2009, 2011). Such seepage-driven pipe formation may explain why pipes have a minimum distance between them, set by a lateral drainage distance from the overpressurized gas zone (Moss & Cartwright, 2010). If near-surface sediment is fluidized, grains may be ejected to the water column and deposited on the PM crater shoulders (Varas et al., 2009). Such sediment ejection in natural PMs is indicated by sonar data from the North Sea indicating massive plumes of suspended sediments above pockmarks (A. Judd & Hovland, 2009). Despite the supporting morphological field evidence, this mechanism remains controversial as it was argued that the initiation of seepage-induced fluidization requires high fluid seepage velocity (i.e., a jet) that cannot be initiated in layered sediments (Cartwright & Santamarina, 2015).
4. *Decompaction*: Two-phase systems consisting of grains and a liquid (with no gas) have shown the spontaneous formation of high permeability fluid escape pipes, forming by decompaction of the granular matrix at the tip of upwelling bubbles ("solitons") comprising buoyant fluids (Räss et al., 2018). When rising pipes reach the surface they form pockmarks. This process requires non-linear rheology of the sediments and has not yet been observed experimentally.
5. *Flow along existing fractures*: gas utilizes existing high permeability faults and fractures to escape from depth (Berndt et al., 2003; Hustoft et al., 2007; Lawal et al., 2023). This process, comprising gas ascent in "pockets," followed by the collapse of fluid-filled cavities or conduits, (also evident in some of our experiments described below), was used to explain observed microseismic events below the Marmara sea (Tary et al., 2012).
6. *Gas hydrate dissociation and volume loss*: This mechanism considers a large body of gas hydrates that accumulates under, and initially inflates (forming a dome), an overlying layer of low permeability sediments. If

the hydrates dissociate due to changes in temperature or pressure, the region may collapse, creating an irregular crater (Riboulot et al., 2016). This is hypothesized as the mechanism forming Type-2 PMs and based on seismic data of pockmarks from the Niger Delta where gas hydrates are abundant. We point out that free gas, even with no gas hydrate source, can also form a dome in soft sediments simply by buoyancy, as observed in offshore New Zealand (Koch et al., 2015), such that the consequent emergence of gas seeps and dome failure can produce Type-2 PMs, as will be shown in the experimental results below.

Finally, we note that while the focus of this work is PM formation by gas seepage, other mechanisms may lead to similar structures: from bottom currents (Klaucke et al., 2018) to feeding of vertebrates (Schneider von Deimling et al., 2023). The ability of these mechanisms to produce pockmark morphology remains a topic of controversy (Schneider von Deimling et al., 2023).

1.3. Nature of Seepage Through Natural Pockmarks

Continuous measurements of pockmark activity in the field are rare, thus the mode of activity of most PMs is uncertain. Observations suggest both continuous seepage (Hovland & Sommerville, 1985; A. Judd & Hovland, 2009) and episodic activity (Field & Jennings, 1987; Franchi et al., 2017; Goff, 2019; Hasiotis et al., 1996; Jedari-Eyvazi et al., 2023; Soter, 1999) exist at different PM locations. Linke et al. (1999) measured many orders of magnitude variability in seepage rates at the Cascadia accretionary complex. Hovland et al. (2002) suggest that most PMs exhibit dormancy as a quiescent period between activities. In some cases, fluctuations in gas fluxes have been observed on a semi-daily basis, often correlated with tides (Schneider von Deimling et al., 2010), or seasonally in response to changes in water temperature (Ferré et al., 2020). However, in other cases, the source of these fluctuations remains uncertain.

1.4. Experimental and Numerical Simulations of Pockmarks and Pipes

Laboratory experiments can aid in determining which mechanisms control the sediment breaching and associated seepage and PM formation, at different conditions. Experiments can also improve understanding of the temporal and spatial evolution of PMs by providing higher resolution, continuous, and more detailed measurements (e.g., optical) than in the field. For instance, seismic reflections include large spatial uncertainty regarding the active pipe geometry, due to past seepage events weakening the adjacent sediment (R. Maia et al., 2016). Temporal resolution is also limited by scarcity of repeated measurements over time in most field sites, whereas continuous observations are easily obtained in the laboratory.

Previous experimental studies of gas-related sediment breaching and PM formation mainly used a homogeneous granular medium (i.e., a single water-saturated granular layer), injecting gas at its bottom (Fauria & Rempel, 2011; Nermoen et al., 2010; Poryles et al., 2016; Ramos et al., 2015; Varas et al., 2009, 2011). For such settings, Varas et al. (2009) showed that if the injection rate is low enough, gas bubbles can ascend through the granular layer intermittently (one at a time). The zone through which the bubbles pass is fluidized, creating a cone-shaped fluidized pipe, where the wide part of the cone defines the crater near the surface (i.e., a Type 1 PM). The transition from capillary gas seepage (at high effective stress) to fracture and Type-1 PM formation (at low effective stress) has been reproduced in laboratory experiments by injecting gas into submersed unconsolidated coarse-grained sediments, and tuning the level of overpressure (and by this the level of effective stress) (Fauria & Rempel, 2011). Investigating further the influence of effective stress on deformation mode, considering the general process of gas seepage from sediments (not specifically PM formation), Z. Sun and Santamarina (2019) found that gas ascends in bubbles when the imposed confining stress is low, while it produces gas-transmitting fractures at higher confinement.

Fewer studies considered layering with a low permeability barrier. Mazzini et al. (2008) injected gas at the bottom of a 2D cell filled with porous granular media overlaid by a thin layer of clay. Gas accumulated beneath the clay until a critical overpressure was reached, leading to (a) doming at the interface between the two layers and (b) lateral migration of the gas along the interface. Further gas injection led to dome fracturing and gas escape. Barry et al. (2012) considered similar layered settings, showing that thin-plate elasticity theory can predict the flexure and doming of the sediment layer versus the applied gas pressure. Specifically, the authors link gas overpressure to dome geometry and material intrinsic mechanical properties (Equation 1 in Ugural (1999)). Barry et al. (2012) found that a small deflection can already cause sediment fracture in natural domes, which may indicate why

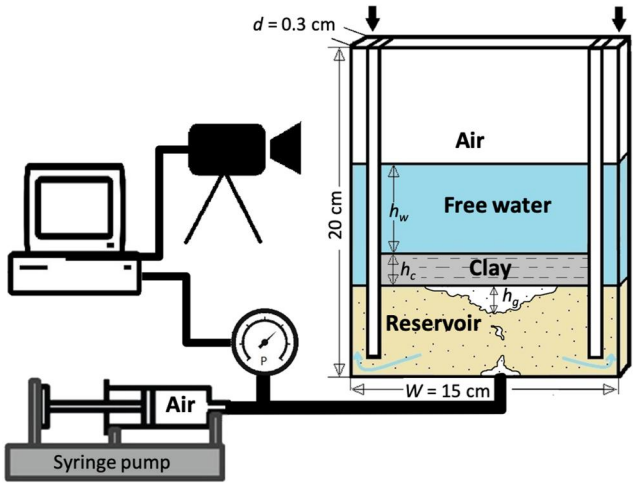

Figure 2. Schematics of the experimental setting: A quasi two-dimensional (2D) cell (thickness $d = 0.3$ cm) made of a Plexiglas transparent box, containing a thin layer of low-permeability granular media (clay) overlaying a more permeable reservoir layer (glass beads), both saturated with water. Gas (here, air) is injected using a syringe pump (where gas pressure is recorded) from a point through the lower face of the cell. Time-lapse images track the sediment deformation. Partitions at sides are used to allow free water drainage (wide arrows), ensuring that overpressure is due to the gas only (avoiding hydrofracturing). We use 2 experimental cell widths, W, 15 and 50 cm.

pockmarks readily form in fine-grained sediments. It was hypothesized that doming represents an early phase of pockmark formation (A. Judd & Hovland, 2009).

1.5. This Study: Open Questions and Our Approach

The above-noted studies advance the understanding of coupled gas-seepage and sediment deformation, and consequent PM formation. Yet, to date, there is no experimental exploration of the *entire* PM formation process—from its initiation, for example, formation of gas conduits from the reservoir, to gas-induced sediment breaching, PM formation, and gas seepage. In particular, we identify the following open questions: What are the mechanical conditions for PM formation? How does PM morphology evolve with time? Is seepage through the PM episodic or continuous? How do PMs tap gas from deeply buried reservoirs? How are different PM morphologies created? What determines the size of a PM? What is the geometrical and mechanical connection between a PM and its feeding pipes?

In this paper, we present a simple experimental setup, that allows us to examine the deformation mechanisms and PM evolution under various settings. Our experimental data, which are in good agreement with theory, explain the formation process of preferential seepage pathways and the episodic, multi-stage, nature of PM generation, and shed light on how different sediment breaching mechanisms result in different types of PMs. Finally, we compare our results to field observations of pockmarks, presenting a simple theoretical analysis that exposes differences and similarities between laboratory and field settings and helps evaluate the applicability of laboratory experiments to natural pockmarks. We discuss the implications of the different spatiotemporal scales, and the intricate codependency between the characteristic spatial and temporal scales.

2. Experimental Setup: Table-Top Pockmarks

We model submarine gas seepage using a rectangular, quasi-2D transparent Plexiglas cell (15 × 20 × 0.3 cm). Filled with two water-saturated granular layers of significantly different grain size and hence permeability, acting as a reservoir overlaid by a seal (Figure 2). All layers are submerged in water. Air is injected through a point at the center beneath the bottom layer by a syringe pump. Images of the injected gas-induced sediment deformation during the experiments are captured using a high-resolution monochrome camera at 10 Hz. The injected air pressure was measured and recorded at 1 Hz at the syringe end. Experiments ran until a stable pockmark was achieved. A clear PM structure was usually formed within 30–60 min, however run-time in most of the experiments did not exceed 75 min, a technical limitation set by the storage capacity. To test the scalability of the experiments, namely the dependence of our results on the system size, a few experiments were repeated with a larger cell (52 × 26 × 0.3 cm), recording images at 5 Hz.

The bottom ("reservoir") layer consists of tightly packed glass beads (RETSCH; diameter range 0.75–1 mm). To ensure a uniform and repeatable packing, after pouring the beads, as they start submerging, the cell was shaken vertically by hand until the beads interlocked and the granular matrix became jammed. The overlaying ("seal") layer consists of natural kaolinite clay (Sigma-Aldrich) poured into the cell in suspension (fluidized in water), left to settle for either 3 or 6 weeks, to test the effect of the degree of consolidation and seal rigidity. Between the sand and the clay layers, we placed a thin (~1 mm) layer of 0.1–0.2 mm glass beads (RETSCH), to prevent downward leaching of the fine clay into the coarse reservoir layer. To ensures that the overpressure that develops in the cell is due to gas overpressure alone, as well as to avoid hydraulic fracturing of the clay by highly pressurized water trapped beneath the low-permeability clay, we install narrow partitions at both sides of the experimental cell. These side partitions allow the water to drain freely releasing water, while preventing gas flow and depressurization. This procedure ensures that the overpressure that develops in the cell is due to gas overpressure alone.

We conducted 24 individual experiments varying the thickness of clay layers (6 values; note that the sand layer thickness was also varied but this parameter is not important), clay settlement duration (2 values), and cell size (2

Table 1
Summary of Experimental Conditions and Results

Test #[a]	Clay (cm)	Sand (cm)	Water (cm)	Settle time, t_s (weeks)	Failure mode[a]	Pockmark type	Run time (min.)
4A	0.7	5.0	5.3	3	D	2	60
3A	0.9	5.1	6.3	3	D	2	58
4B	0.9	7.0	5.2	3	P	1	52
5A	0.9	7.0	5.2	3	D + P	1	30
5B	0.9	7.0	5.2	3	D + P	1	30
3E*	1.0	5.0	5.2	3	P	1	60
2A	1.4	7.5	6.1	3	P	1	60
2B	1.4	7.1	5.6	3	D + B	2	33
3B	1.6	4.8	5.4	3	P	1	22
4C	1.6	7.0	5.2	3	P	1	57
2E*	1.6	5.0	16.9	3	P	1	43
2C	2.2	7.0	5.0	3	B + P	1	56
2D	3.8	7.0	5.2	3	P	1	43
3C	3.8	4.9	5.3	3	P	1	54
4D	5.0	5.0	5.3	3	P	1	54
4E*	10.0	6.8	5.2	3	P	1	130
1A	0.7	7.0	6.4	6	D	2	40
1B	1.2	7.1	5.9	6	D + P	2	45
5E*	1.7	5.0	16.8	6	D	2	60
1C	1.8	6.7	5.2	6	B	1	35
1E*	2.0	7.2	10.3	6	B	2	66
5C	2.2	5.4	5.5	6	B	1	73
5D	2.2	5.3	5.5	6	B	1	83
1D	2.5	5.5	6.5	6	B + P	1	60

[a]* = Wide experimental cell (W = 50 cm); in all other cases we use W = 15 cm. [a]D = Doming; B = Brittle; P = Plastic.

values). The experimental setting as well as the emerging deformation mode and pockmark type of each experiment are summarized in Table 1, where the experimental parameters and their values are listed in Text S2 in Supporting Information S1. The repeatability of the experiments was verified based on two sets of runs with similar initial experimental conditions. Indeed, each set resulted in similar deformation modes (4B, 5A, and 5B; 5C and 5D, see Table 1). However, the specific details of the sediment deformation patterns and pressure at failure slightly differed, as expected due to unavoidable randomness in packing. We classify the PM type visually according to its geometry at the end of the experiment: (a) Type-1—regular, conical, U-shaped depressions that are empty of sediments; and (b) Type-2—irregular depressions hosting faulted and deformed sediment.

3. Experimental Results

3.1. Modes of Seal Breaching and Gas Seepage

In all experiments, we observed similar stages of gas *seepage*: (a) gas ascended through the (sand) reservoir and accumulated under the overlaying seal (clay) layer; (b) pressure progressively builds up with the continuous gas injection and accumulation, until the threshold for seal failure is met (Figure 3); (c) the gas then seeps upwards and finally a pockmark is formed. However, the seal *failure* mode, which depends on clay layer thickness, h_c, and duration of clay settlement before injecting the gas, t_s (controlling its rigidity), differed among experiments, ranging from (a) doming, where the sealing layer bends and later breaches, allowing the escape of ascending gas through Mode I fractures; to (b) brittle, where ascending gas pressure induced shear (Mode II) faults which served as pathways for gas escape; to (c) plastic, where gas bubbles buoyantly rose through liquefied sediments.

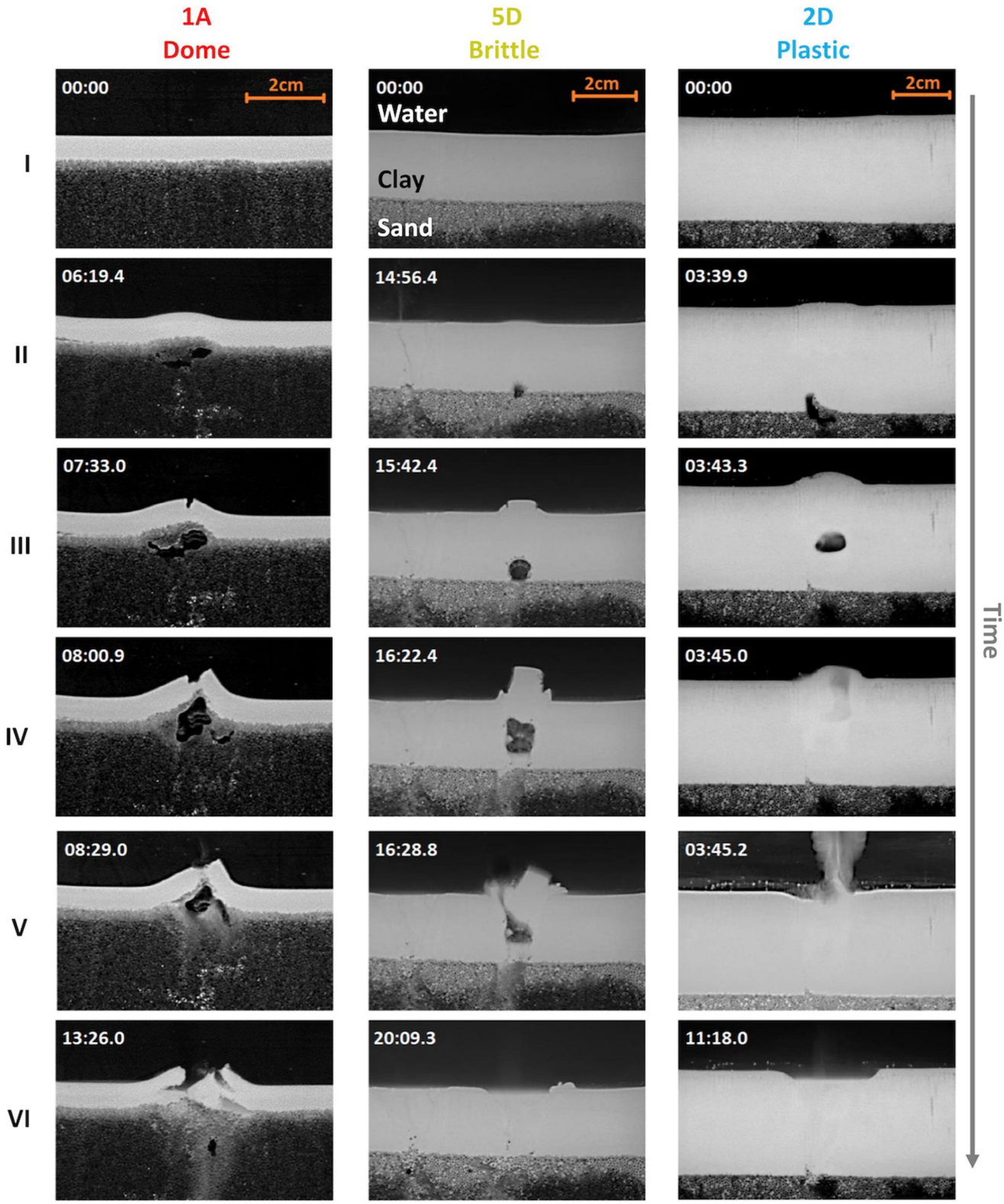

Figure 3.

Doming was the dominant mechanism in experiments where the clay was thinner and/or more rigid, and progressed according to the following stages (e.g., experiment #1A in Figure 3 and Movies S1 and S2): (a) pressure build up in the interlayer gas pocket; (b) the overlying clay layer bends to form a dome; (c) the dome fractures by Mode I (opening) fractures and breaches; (d) gas enters the fractures of the breached dome, widening them and seeps through; (e) The dome is deflated, causing clay blocks to collapse inward; (f) gas continues to seep episodically through the gaps between the clay blocks, progressively disintegrating and eroding them, resulting in suspension of clay particles. Eventually, a shallow crater is created hosting collapse blocks, namely a Type-2 pockmark. In most cases, stages a–c take several minutes. Complete deflation and internal collapse of the dome (stages e–f) require multiple gas seepage episodes. Blocks tend to interlock and can be rotated and displaced, such that a subsequent breaching of the dome and collapse requires an additional gas pressure buildup.

Brittle deformation was the dominant mechanism in experiments with intermediate thickness, rigid clay layer, and was observed to evolve in the following manner (e.g., experiment #5D, Figure 3 and Movie S3): (a) pressure builds up to a critical point (see pressure evolution in Text S1 in Supporting Information S1); (b) gas invades the clay layer by displacing and compressing it to create a "piston" at the base of the clay layer, in agreement with the prediction in Cathles et al. (2010). A cavity (gas bubble) starts to form within the clay, creating a mound at the top of the clay layer; (c) the gas bubble continues to grow, mostly upwards, and two sub-vertical faults appear (more noticeable at the top part of the clay), defining a free block (plug); (d) the gas uplifts the clay block, in a piston-like motion; (e) then, gas seeps through one of the faults, along which the clay disintegrates and liquefies; (f) with continued seepage, the plug disintegrates entirely and a U-shaped Type-1 PM forms.

Plastic deformation of the clay was dominant in experiments in which the sealing layer was relatively thick, for example, #2D (Figure 3) and #4E (Figure 4), and in which the clay had less time to solidify. Deformation generally evolved in the following manner (experiment # 2D in Figure 3 and Movies S4 and S5): similar to the case of the brittle deformation, (a) gas invaded the clay layer by displacing it to create a "piston" (Figure 4), after which (b) a bubble starts to grow within the clay at the edge of the piston (Figure 4a), forming a mound at the top of the clay layer. Then, (c) the bubble detached from the main gas reservoir at the sand-clay boundary and migrated upwards, distorting the clay (Figure 4a); (d) the bubble continued to migrate upwards toward the top of the clay layer, while the clay rearranges around the bubble; (e) the bubble erupted at the top of clay layer, dragging and suspending clay particles (Figure 4b); (f) after a series of repeated episodes of bubble eruption a significant amount of clay was removed such that a noticeable U-shaped crater that is, Type-1 PM formed, resembling the one formed by the plug-like brittle deformation. This stream of individual bubbles progressively weakened the clay to create a damage zone (pipe) within it, serving as a conduit for further bubble migration (Figure 4c). Bubbles continuously suspend clay from the pipe such that with time the outline of the damaged pathway or pipe becomes noticeable (Figure 4d). The migration of the bubble through the clay layer (stages b-e) occurred within ~5–10 s, depending on the clay layer thickness (Figures 4a and 4b).

We also observed mixed deformation modes: (a) doming/brittle deformation mode when a fault-bounded plug was developed in a dome (e.g., #2B); (b) doming/plastic deformation when ascending gas bubbles seep through the breached dome (e.g., #5A and 5B); and (c) brittle/plastic when an existing fault, serves as a conduit for packets of gas to escape as elongated (non-spherical) bubbles (#1D, cf. Figure 5).

3.2. Pockmark Formation and Episodic Seepage

Our experiments show that following the initial seal breaching, gas does not flow continuously upwards, unlike in ordinary percolation. Instead, flow pathway and pockmarks developed progressively during episodic seepage

Figure 3. Snapshots showing the main stages of gas escape through a seal (gas accumulation at the seal-reservoir interface, seal breaching, gas seepage through the seal, and pockmark initiation) in three representative experiments of increasing clay layer thickness h_c (see Table 1 for details). The three experiments exemplify the three main deformation mechanism: (Left column) *Doming* (experiment #1A, $h_c = 0.7$ cm) is initiated by gas accumulation at the seal-reservoir interface. When the accumulated gas causes large enough dome deflection, the dome is breached by Mode-I (open) fracturing, leading to the development of a Type-2 pockmark (see also Movie S1); (Middle column) *Brittle* deformation (#5D, $h_c = 2.2$ cm). Gas accumulation at the reservoir-seal interface produces a mound in the seal, followed by Mode-II sub-vertical faulting. Seepage then occurs through these shear faults, bounding an uplifted plug, leading to the development of a Type I pockmark (see also Movie S3); (Right column) *Plastic* deformation (#2D, $h_c = 3.8$ cm), shows gas transmitted to the surface by ascending gas bubbles, leading to the development of a Type-1 pockmark (see also Movie S4). In each snapshot (only shown is the central part of the cell) the lower part (dark gray) is the top of the sand layer, and the middle part (light gray) is the clay (seal) layer which is overlaid by water (black). Rows I–VI correspond to progressive deformation stages since injection started (I); time (min:sec) since injection shown in upper left corner.

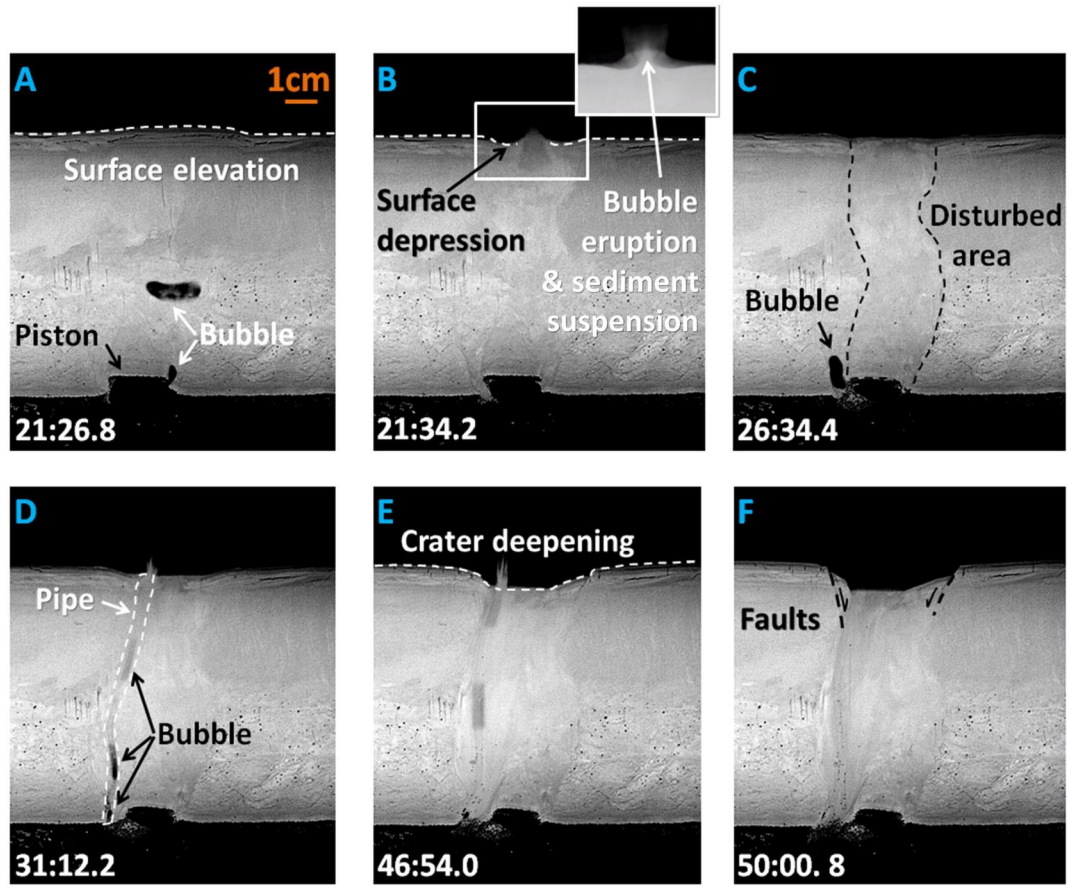

Figure 4. Experimental snapshots showing the development of a plastically failing PM, with a feeding pipe (Experiment #4E; see Table 1 and Movie S5): (a) a piston forms with a bubble rising from its edges; (b) bubbles escape from the surface, ejecting suspended material to the water, creating a surface depression (c) bubbles initially escape from both sides of the piston, and the whole area above the piston is disturbed; (d) sequential bubble ascent creates a pipe bordering the piston; (e) episodic bubble rise through the pipe removes more material at the crater, whose borders are defined by the disturbed area; and (f) continuous development of the Type I pockmark by the collapse of the walls via faulting, interspersed by bubble escape, leading to widening of the disturbed area. The active episodes are interspersed by quiescent periods (Movie S5). Each snapshot shows the central part of the experimental cell. The lower part (black) is the top of the sand layer, and the middle part (light gray) is the clay layer which is overlaid by water (black). Time (minutes:seconds) since the start of gas flow is marked at the lower left corner of each snapshot.

events. The intermittent nature of the deformation and seepage is also evident from the pressure temporal variations: gas pressure fluctuated in association with the evolution of the PM (cf. Text S1 in Supporting Information S1). We emphasize that the gas pressure measured in the inlet (syringe) is not associated with the gas pocket pressure after its detachement from the main gas reservoir and advancement into the seal layer. The evolution of PM morphology versus number of seepage events N for each of the main deformation modes is shown in Figure 6.

3.2.1. Type-2 Pockmarks

In cases where the seal was initially deformed into a dome-shaped structure (that later collapsed), a complete Type-2 PM depression developed as a result of a sequential seepage through the debris of the collapsed dome (Figure 6 #1A, $N = 7$–25). Type-2 PM seeps did not always occur from the same breach between adjacent blocks: gas was able to seep from different locations within the same PM, depending on the PM size and the number of blocks. Type-2 PMs either form from a wide dome that disintegrated into multiple blocks, or from small adjacent domes that merged into a single large PM (Figure 6 #1B). As seepage continued, the blocks within Type-2 PMs were observed in some cases to gradually disintegrate, whereas in other cases PM morphology remained relatively unchanged.

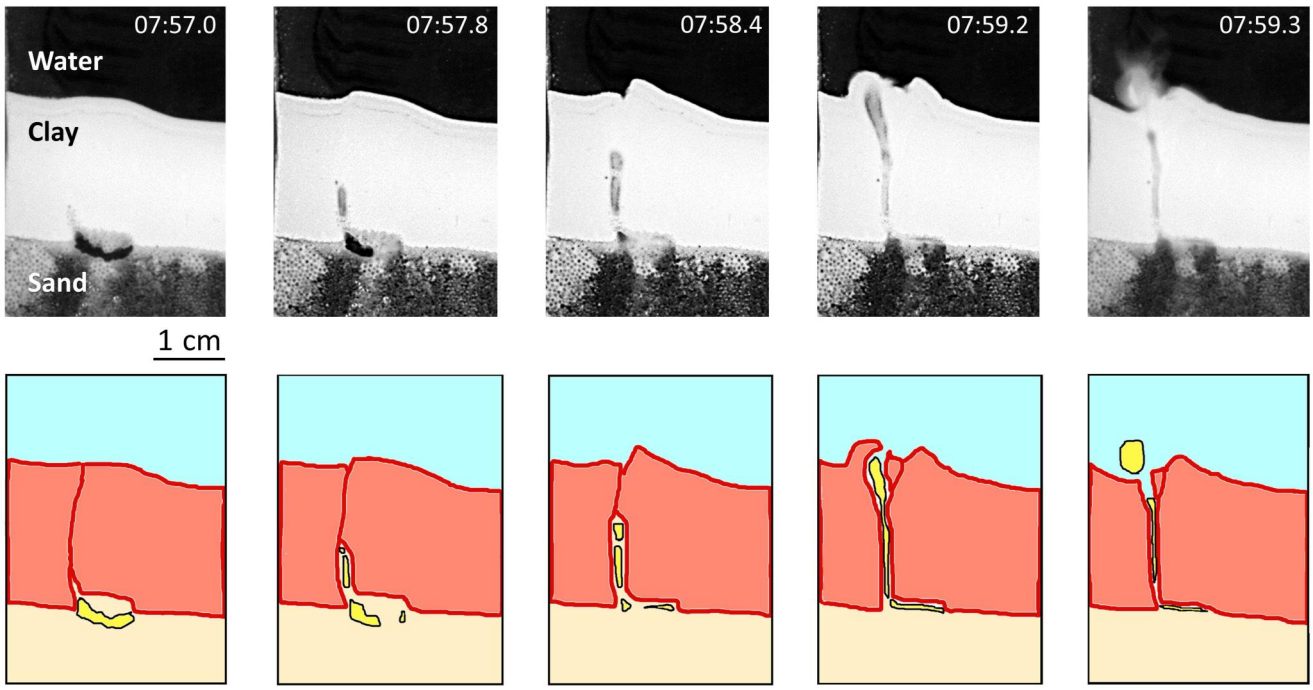

Figure 5. Experiment #1D shows a fracture and gas-filled, elongated, bubbles ascending through it. For clarity, each experimental image (top row) is accompanied by a schematic reconstruction (bottom row). The clay layer appears in white (red in the schematic), between the bottom reservoir layer in gray (yellow) and water above in black (turquoise). Bubbles appear in gray/black (yellow). Time (minutes:seconds) since the start of gas flow is marked at the upper right corner of each snapshot.

3.2.2. Type-1 Pockmarks

When the seal breached in a brittle or plastic manner, gas bubbles ascended through a Mode II fault or through the bulk sediment, with each seepage event deepening an erosive crater toward the development of a complete Type-1 PM. For instance, in experiments #1C and #2D in Figure 6, the first event ($N = 1$) is seen to only slightly modify the topography, where as seepage continues clay is progressively removed from the PM zone by its suspension into the water column, making the PM shoulders clearly evident ($N = 7$; see also Figure 4b). Further events ($N = 7$–15) make the clay below the pockmark along the seepage route looser such that it remains in suspension, until finally ($N = 25$ in Figure 6), most of the clay is removed all the way down to the sand layer, creating a cone-shaped Type-1 PM. This makes the gas pipe and PM geometry interrelated: as the pockmark gets deeper it erodes and shortens the pipe that feeds it.

In early stages, Type-1 PMs initially deepen at a relatively uniform rate, that is, depth D increased linearly with N (Figure 7a), irrespective of clay layer thickness h_c. The deepening rate accelerated once $D \sim 0.2$–$0.3h_c$, especially for thicker clay layers. Eventually, the PM traverses the entire clay layer, $D \approx h_c$. Occasionally, PM depth decreases (Figure 7a) due to suspended sediment or sediment from the PM rim that is falling back to the PM. The PM width L progressively increased with seepage cycles, via collapse of the PM walls (Figure 7b; Movie S4). This collapse was episodic, that is not every seepage event that caused widening of the PM also resulted in collapse and deepening (Figure 7c); collapse and deepening only occurred once the PM walls reached a critical angle. This is probably due to the hysteresis arising from the difference between static and dynamic angles of friction in granular media, that is, in sediments (Perrin et al., 2019; Volfson et al., 2003).

In many experiments, the seepage location changed with time, creating several PMs (#1B in Figure 6 and Movie S3). The number of seepage locations was inversely proportional to the clay thickness, irrespective of the type of seepage mechanism and domain size. When PMs were close to each other they merged to form a single wide PM. While our thin, quasi-2D experimental domain promotes PM merging by limiting the seepage location to a narrow line (vs. a surface in 3D domains), field observations of PM merger (Schattner et al., 2016) suggests that this is a viable mechanism also in more complex, 3D domains.

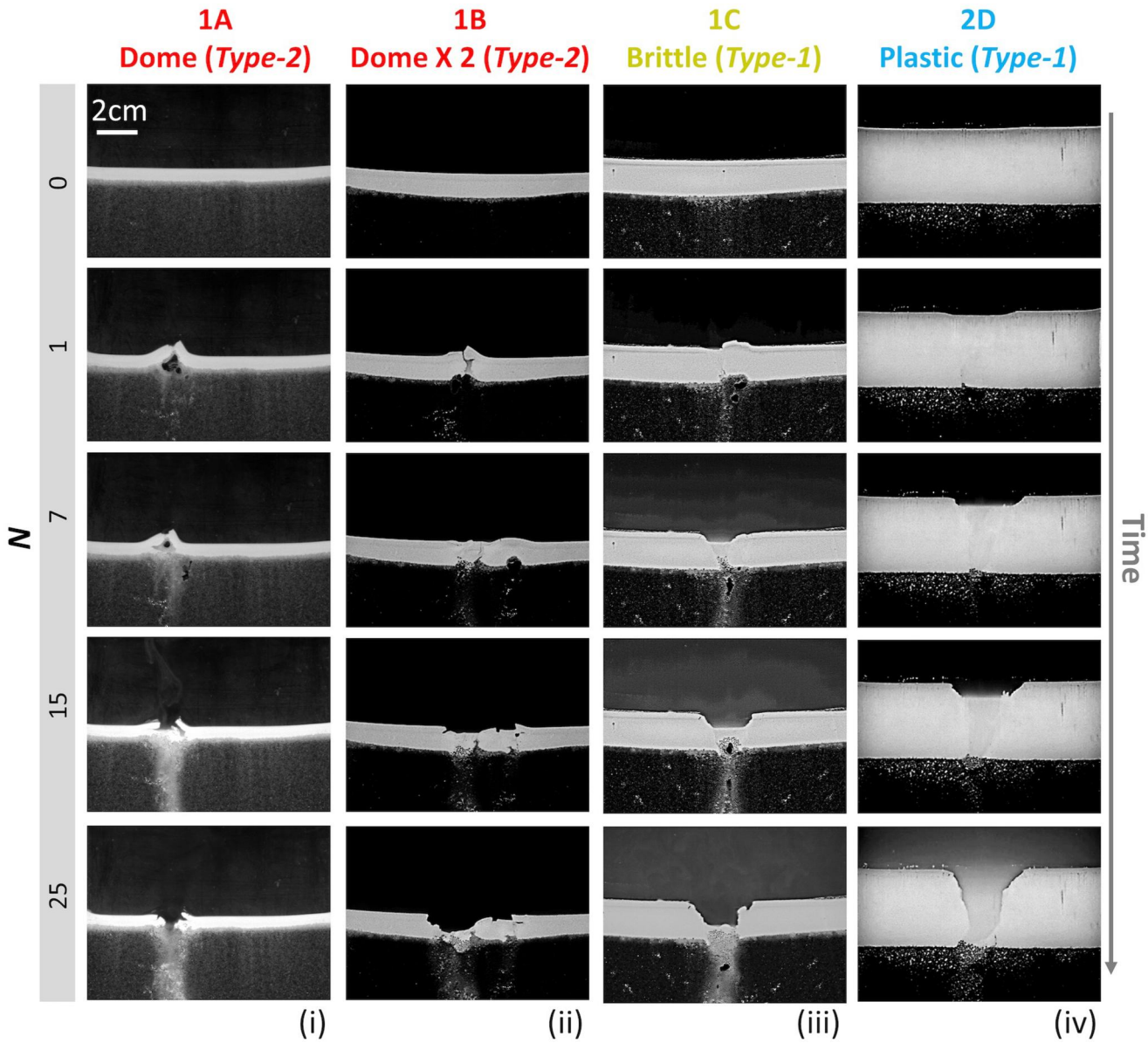

Figure 6. Experimental snapshots of pockmark development as a function of the number of seepage events, *N*, in four selected experiments with increasing clay thickness, h_c, exhibiting a transition in deformation mechanisms and final PM type. In each snapshot, the lower part (dark gray to black) shows the top of the sand layer, and the middle part (light gray) shows the clay (seal) layer which is overlaid by water (black). (i) Experiment #1A ($h_c = 0.7$ cm): Doming and breaching by the fracturing of the dome and development of Type-2 pockmark; (ii) #1B ($h_c = 1.2$ cm): Doming and breaching by the fracturing of a first dome, which is followed by the development of a second dome, its breaching and eventually development of a single Type-2 pockmark; (iii) #1C ($h_c = 1.8$ cm): Breaching by faulting, plug uplift, and development of Type-1 pockmark; (iv) #2D ($h_c = 3.8$ cm): Breaching by plastic deformation (liquefaction) around ascending gas bubble and development of Type-1 PM.

3.3. Experimental Phase Diagram of Pockmark Formation

The experimentally observed deformation mechanisms and resulting structures as a function of the clay layer properties—clay thickness, h_c, and settling time, t_s, is presented as a phase diagram in Figure 8 (see details of the experimental settings in Table 1). This diagram demonstrates the dependence of the deformation mode on the clay properties: (a) *Domes* occurred only in very thin layers ($h_c < 1$ cm) in the narrower experimental boxes ($W = 15$ cm; used for most experiments), and at a wider range of clay thickness ($h_c < 2$ cm) in the wider cells ($W = 50$ cm); (b) *Brittle deformation* was dominant in thicker and stiffer layers (that settled longer, $t_s = 6$ weeks); and (c) *Plastic deformation* (by bubble migration) was observed in thicker, softer ($t_s = 3$ weeks) clays.

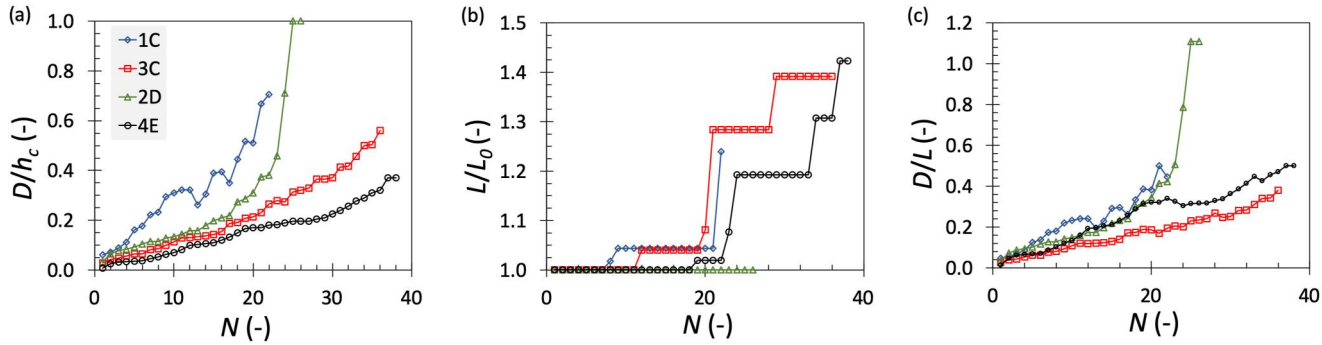

Figure 7. Quantitative analysis of the evolution of pockmark geometry versus the number of seepage events, N, for experiments showing different deformation modes: brittle in #1C and plastic in #3C, #2D, #4E. (a) Pockmark depth, D, normalized by the clay layer thickness, h_c; (b) Pockmark width, L, normalized by its initial value, $L_0 = L(N = 1)$; (c) Pockmark aspect ratio D/L.

4. Theoretical Prediction of Deformation Mechanisms

This section provides a predictive quantitative analysis of the mechanisms for seal deformation and breaching observed experimentally: doming, brittle, and plastic deformation. The parameters and the values used for the calculations are provided in Text S3 in Supporting Information S1. In our experiments, the gas injected into the bottom of the coarse grained (reservoir) layer, rises through it and accumulates under the overlaying clay. Due to the large capillary pressure required to invade the small pores in the clay, gas remains trapped as a gas pocket, also serving as a "capillary barrier" which blocks the upwards flow of water (Morel-Seytoux, 1993). The gas overpressure driving the deformation, $\Delta P(z) = P_g(z) - P_w(z)$, is defined as the difference between the pressure of the gas pocket and of the water at height z, $P_g(z)$, and $P_w(z)$, respectively. In computing it, we assume hydrostatic pressure distribution in the water column, as the side valves in our setup enable rapid release of water pressure to maintain hydrostatic conditions (Figure 2). We stress that, even in a fully hydrostatically balanced system, buoyancy forces can create overpressure (Osborne & Swarbrick, 1997). To illustrate this, consider a gas pocket of height h_g disconnected from the syringe (Figure 2). At the base of the gas pocket, the gas pressure is equal to that in water-saturated (gas-free) regions at a similar depth. Inside the gas pocket, the pressure decreases with elevation as $-\rho_g g h_g$, that is, more gradually than in the water phase (P_w decreases as $-\rho_w g h_g$), where ρ_w and ρ_g are the density of water and gas respectively, and g is the gravitational acceleration. This implies that the gas overpressure at the bottom of the clay is proportional to the height of the gas pocket, $\Delta P = (\rho_w - \rho_g) g h_g$. As the volume of the trapped gas pocket increases and h_g grows, ΔP at the top of the pocket increases until it suffices to deform the seal. It is possible that in our experiments there was a connected gas pathway from the syringe to the base of the seal; this could not be deduced from image analysis. In such a case, gas overpressure would exceed that arising from buoyancy (hydrostatic) forces alone.

The stress in the clay is computed assuming lithostatic distribution, that is, that the clay grains support their own weight plus the weight of the water, $\sigma_{v,\mathrm{lit}} = \rho_c h_c g + \rho_w h_w g$, where ρ_c is the saturated clay density, h_c is the clay thickness, and h_w is the water depth from the surface to the top of the clay layer (Figure 2). Thus, the effective stress at the bottom of the saturated clay layer is

$$\sigma'_v = (\rho_c - \rho_w) h_c g. \quad (1)$$

Clay deformation in our experiments occurs much faster relative to the flow and pressure relaxation of water in the clay, such that we consider undrained conditions (in contrast to the assumption in Cathles et al. (2010)). This can be justified by scaling: we observe clay deformation within seconds—the time for a bubble to traverse the clay layer by deforming it (e.g., see Figure 3, right column). The timescale for the flow across the layer can be evaluated from Darcy's law. We note that clay permeability can span a large range, $10^{-20} - 10^{-14}$ m^2, (Chapuis & Aubertin, 2003; Neuzil, 1994); using the higher value of 10^{-14} m^2 provides the lower bound for the flow timescale. The gas pressure difference between the bottom and the top of the clay was not measured; we use instead the upper bound for gas pressure in the experiments, ~2 kPa (Figure S1 in Supporting Information S1). Assuming porosity of 0.1 and $h_c = 10$ cm, provides an upper limit of ~1 μm/s for the velocity of water drainage

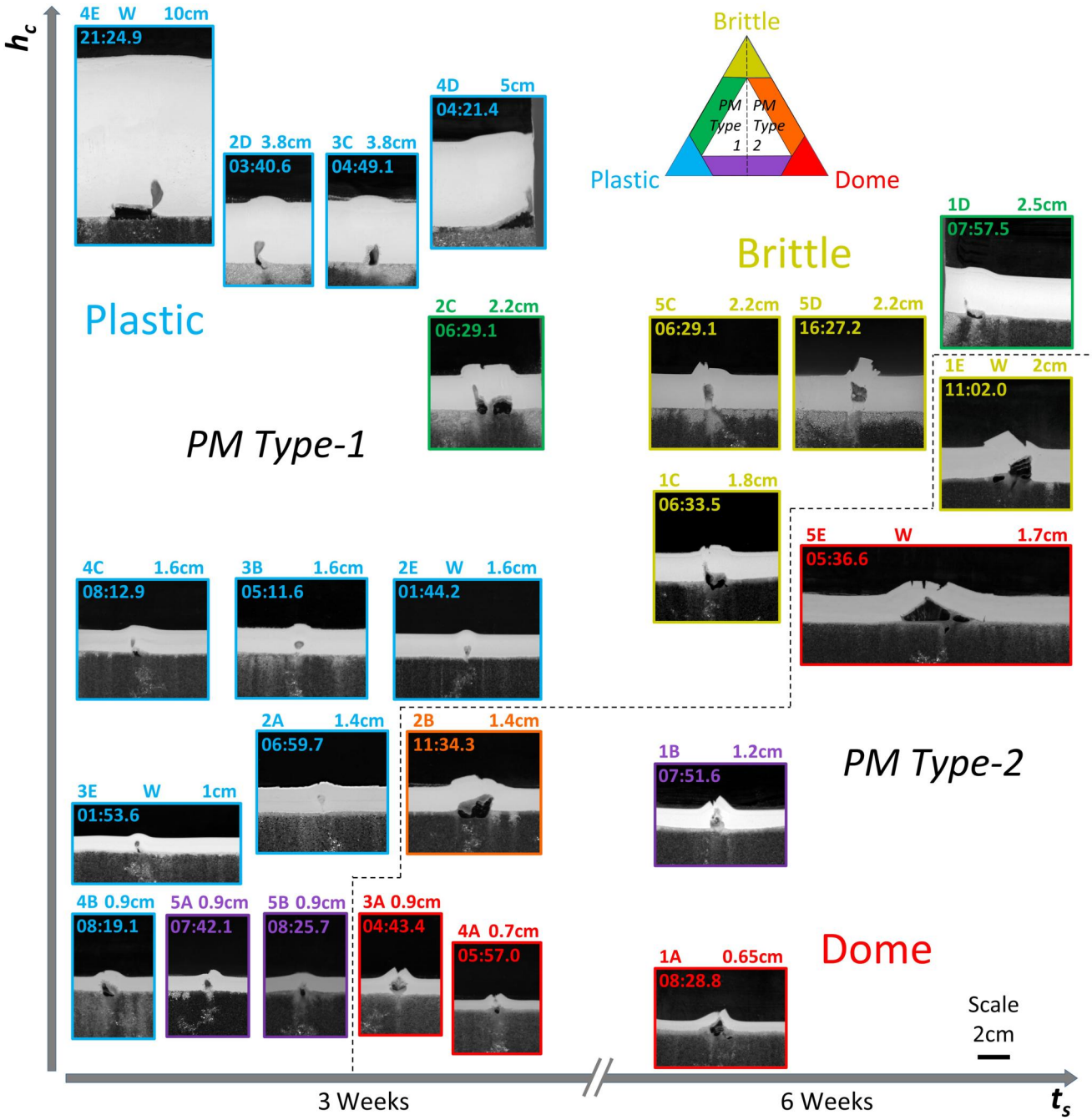

Figure 8. Experimental phase diagram of deformation mechanisms versus settings in terms of clay thickness, h_c, and settling time, t_s. Final pockmark geometry is shown for 14 experiments, including (top row) the experiment number (left), "W" if the wider (50 cm) cell was used, h_c (right), and the time elapsed since seepage initiation (hh: min), below. The diagram is divided into PM Type-2 domain and Type-1 domain, where the boundary is marked by a dashed line. The axes are not up to scale, that is, snapshot locations are relative: higher indicates larger h_c, and left and right correspond to t_s is 3 or 6 weeks, respectively. Snapshots are color-coded by formation mechanism (see the phase triangle): doming (in red); brittle plug development and seepage through fractures (yellow); plastic deformation by bubbles (blue); mixed doming/plastic mode (purple); mixed doming/brittle (orange); mixed brittle/plastic (green).

from the clay, corresponding to $\sim 10^5$ s (across a distance of $h_c = 10$ cm),4 orders of magnitude longer than the time of deformation. This justifies our undrained assumption.

In the Sections below, we derive theoretical expressions for the conditions required for each mode of clay deformation, relying on the "critical state soil mechanics" theory (Wood, 1991). Details and parameter values are

provided in Text S2 in Supporting Information S1, relying on the following literature: Ouyang and Mayne (2018), Atkinson (2017), Xu et al. (2018), Marcuson and Wahls (1972), Mukabi and Hossain (2011), Ishihara (1996), Chapman and Godin (2001), Snieder and Beukel (2004), and Athanasopoulos (1993).

4.1. Dome Breached by Fracturing

Consider an elastic dome, breached by a fracture when deflection becomes large enough (as in experiments # 1A, 5E, 4A, 3A in Figure 8). The conditions for this mechanism are evaluated using analytical expressions from the three-point beam flexure theory (Bower, 2009). This theory computes the deformation of a rectangular beam loaded at its middle while supported at its edges. Beam failure occurs when the strain at its outer (curved) edge exceeds its tensional strength. This scenario is used as an approximation for our quasi-2D experiments, where the gas pushes the clay seal from below approximately at its center (experiment #1A in Figure 3, and # 1E, 5E in Figure 8). The pressure required to fracture in tension a beam (dome) of length a (Figure 9a) by a pressure ΔP_{dome} is (Bower, 2009)

$$\Delta P_{\text{dome}} = \frac{2}{3}\frac{h_c{}^2\left(\sigma'_v + T_0\right)}{Wa} \tag{2}$$

where T_0 is the clay tensional strength and W is the cell width.

4.2. Brittle Deformation

Brittle failure occurs in our experiments via formation of a block bordered by faults ("plug"), for example, see experiment # 5D in Figure 3 and #1E, 1C, 5C in Figure 8. The first step in creating a plug is the formation of a gas "piston" (see elaborated discussion in Section 4.3.1). In brittle layers, upward piston motion produces sub-vertical side faults that delineate the plug. The plug is then lifted by frictional sliding along the faults (#1A, 1C, 5C in Figure 8). The fractures surrounding the plug—which is often tilted—act as gas escape pathways.

The gas overpressure required to induce faulting that creates and lifts a plug, ΔP_{plug}, must overcome two forces: one to create faulting in the clay layer, F_{frac}, and another to slide the plug upwards on the 2 faults delineating it, F_{slid}.

$$\Delta P_{\text{plug}} = \max\left(F_{\text{frac}}, F_{\text{slid}}\right)/A_b. \tag{3}$$

Here $A_b = dl$ is the area of the plug base, d is the spacing between the plexiglass walls, and l is plug length (Figure 9b). The shear force required to create a fault is related to the gas pressure via $F_{\text{frac}} = A_b \Delta P_{\text{frac}}$, which in turn can be obtained from the criterion for fracturing of clay by shear (Marchi et al., 2014),

$$\Delta P_{\text{frac}} = \sigma'_3 + nc_u = \sigma'_v + nc_u. \tag{4}$$

Here n is an empirical coefficient of order unity (Atkinson et al., 1994). In Equation 4 and the calculations hereafter, we assume $\sigma'_3 \approx \sigma'_v$. The undrained shear strength of clay is (Equation 8 in Mayne (2001))

$$c_u = 0.5\sigma'_v \sin(\phi)(OCR)^{\gamma}, \tag{5}$$

where ϕ is the undrained friction angle, OCR is the overconsolidation ratio, and σ'_v is the effective stress, given by Equation 1 for clay seal base. The exponent γ is found empirically (Z. Sun & Santamarina, 2019). For the selection of parameter values, including ϕ, n, γ and OCR, see Text S2 and Table S1 in Supporting Information S1.

The sliding force F_{slid} in Equation 3 is computed as the sum of the following forces: (a) frictional resistance to the sliding of the plug against its two bordering faults (assumed to be sub-vertical), $2\sigma'_v \mu_c h_c d$; (b) frictional resistance with the cell walls, $2\sigma'_v \mu_w h_c l$; and (c) the force to lift the plug weight, $\sigma'_v A_b$:

$$F_{\text{slid}} = \sigma'_v\left(2\mu_w h_c l + 2\mu_c h_c d + dl\right) \tag{6}$$

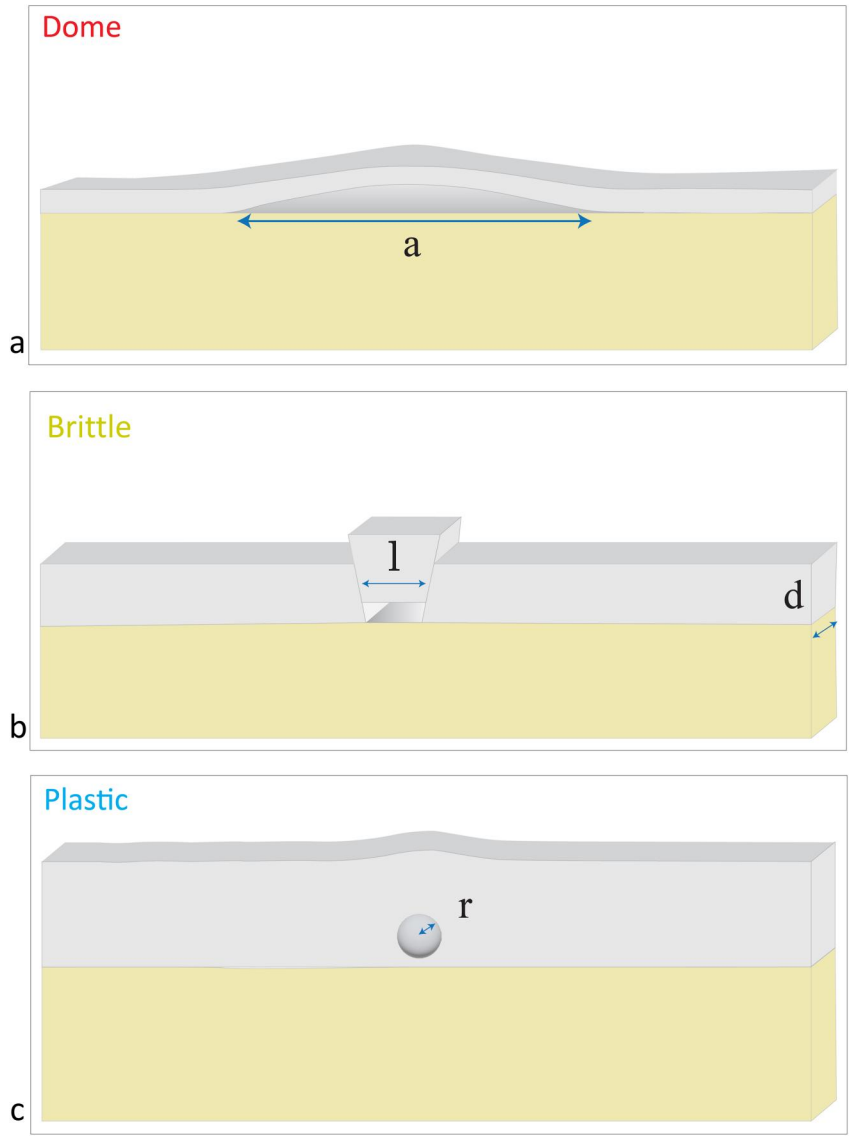

Figure 9. Characteristic length scales used in the analysis of the different seal breaching and deformation modes: (a) gas pocket forming a dome (dome width: *a*); (b) faults creating a plug (of base length *l* and thickness *d*), lifted by a gas pocket; (c) gas bubble (of radius *r*) rising within the clay.

where μ_c and μ_w are the clay-clay and clay-wall friction coefficients, respectively (see Text S2 in Supporting Information S1). Substituting F_{frac} and F_{slid} into Equation 3 provides the critical pressure for brittle deformation,

$$\Delta P_{\text{plug}} = \max\left[\sigma'_v + nc_u, \sigma'_v\left(2\mu_w\frac{h_c}{d} + 2\mu_c\frac{h_c}{l} + 1\right)\right]. \quad (7)$$

4.3. Plastic Deformation

The third possible mode of seal failure is the creation of a cavity by plastic deformation (9C). This cavity may form by the rise of either a "piston" or a gas bubble (Figure 4a). In thin clays (#4C, 2E, 3B in Figure 8) bubbles are created at the bottom or middle of the clay layer. In thicker clays bubbles are often generated from tips of a flat piston (Cathles et al., 2010) that first yields into the clay (Figure 4; Figure 8 #4C, 4D). The conditions for the different stages of plastic deformation are computed below.

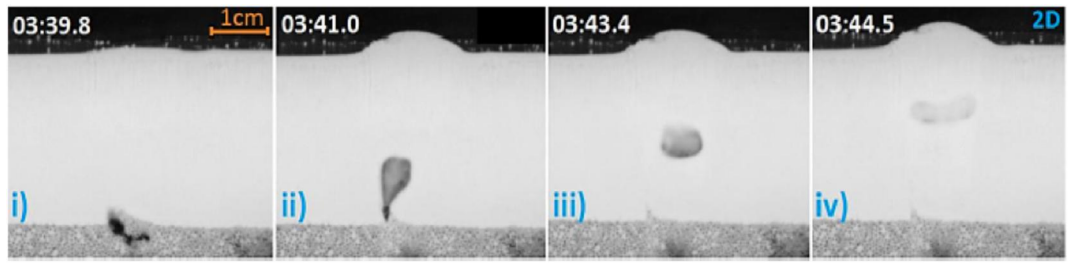

Figure 10. Four stages of bubble migration in clay (experiment #2D): (i) Gas invasion, (ii) bubble vertical growth and detachment, (iii) rounded bubble migration, (iv) bubble flattening due to its movement upwards. In each snapshot, the lower part (dark gray) shows the top of the sand layer, and the middle part (light gray) shows the clay (seal) layer which is overlaid by water (black). The time elapsed since seepage initiation (hh:mm) appears in the upper left corner.

4.3.1. Piston Formation

In some of the experiments with thick seals, a "piston" developed above the large gas pocket pushing into the clay seal. The piston, shaped by the capillary forces associated with interfacial tension, has a relatively flat top and limited width. Cathles et al. (2010) hypothesized (a) the development of such a piston; (b) that the piston dimensions depend on the pore size distribution; and (c) the rising piston will liquefy the sediments above it, allowing it to accelerate upwards. Our experiments indeed demonstrate that in some cases a piston is created, and our calculations below predict that it will liquefy the clay above it. However, we do not observe an acceleration of the piston; instead, we observe that the piston comes to a halt, and the trapped gas escapes via bubbles emanating from its edges (Figure 4). Bubble formation at the edges is aided by stress concentration at the sharp edges of the piston.

4.3.2. Bubble and Cavity Formation

The pressure required to form a gas-filled cavity (bubble or piston) in the clay is

$$\Delta P_{\text{cavity}} = \sigma'_v + 1.3c_u\left[1 + \ln\left(\frac{E}{2c_u(1+\nu)}\right)\right], \tag{8}$$

where E and ν are Young's modulus and Poisson ratio of the clay (Z. Sun & Santamarina, 2019). Equation 8 implies that ΔP_{cavity} always exceeds the liquefaction threshold, $\sigma'_v + c_u$, supporting the hypothesis that clay will be liquefied around the cavity. Liquefaction allowing bubbles to ascend by pushing the clay in front of them was observed experimentally by Varas et al. (2011); Ramos et al. (2015). Furthermore, as both σ'_v and c_u are proportional to clay thickness h_c (Equations 1 and 5), Equation 8 suggests that the pressure of the bubble or piston also increases with h_c, as confirmed by our experimental data (Figure S2 in Supporting Information S1).

4.3.3. Bubble Ascent

A gas bubble will continuously grow in place until the buoyancy force overcomes the drag force, allowing it to ascend (Figure 10). Bubble ascent requires an additional force (beyond that required for bubble formation and liquefaction) to overcome the drag force resisting the bubble motion within the clay. The drag force is estimated here via dimensional analysis,

$$F_d = kc_u\pi r^2, \tag{9}$$

where r is bubble radius and k is an empirical parameter. The buoyancy force acting to lift the bubble is computed from the weight of the submerged clay it displaced, of volume similar to that of the bubble, $4/3\pi r^3$:

$$F_b = (\rho_c - \rho_w)\frac{4}{3}\pi r^3. \tag{10}$$

Once the bubble reaches a critical radius, $F_b = F_d$, and it starts to rise. The critical bubble radius to overcome the drag is computed from the above together with Equation 5,

$$r_c = \frac{3kc_u}{4(\rho_c - \rho_w)} \approx 0.13kgh_c(OCR)^{\gamma}. \quad (11)$$

The factor 0.13 in Equation 11 arises from substituting into Equation 5 the definition of σ'_v from Equation 1, together with $\phi = 20°$ (Table S1 in Supporting Information S1). Equation 11 predicts a dependence between the critical bubble size and layer thickness h_c, in agreement with our experimental observations (Figure S2 in Supporting Information S1). We note that Equation 11 relies on the assumption of a spherical bubble, whereas in many cases bubbles were distorted during ascent, for example, see Figures 5 and 10. This, together with the limited number of experimental data points, prevented a reliable estimate of k from our data.

4.3.4. Pipe and Pockmark Formation by Bubble Ascent

Bubbles ascend while liquefying the sediment in front of them. This leaves a record of the gas passage in the form of a liquefied pathway within the clay (Figure 4), providing an easier pathway for subsequent bubble ascent (by reducing both ϕ and OCR, and hence c_u, cf. Equation 5). Repeated occurrence of this mechanism creates a localized gas pipe (Figures 4d and 4e), of a width that is correlated with the bubble dimensions. Each escaping bubble also deepens the crater (Figures 4e and 47a). As the crater walls repeatedly collapse by faulting and sliding (Figure 7b), it forms a pockmark (Figure 4f) of increasingly larger depth to width ratio (Figure 7c). In some cases when fractures form, they serve as pipes for venting elongated bubbles (that fit the fracture width, cf. #1D in Figure 5), a mixed brittle/plastic deformation mode (e.g., #2C in Figure 8).

4.4. Transition Between Failure Mechanisms

Following a gas pocket buildup at the base of the clay seal, gas escapes in our experiments by either (a) fracturing an elastic dome; (b) brittle deformation, as a plug delineated by faulting; or (c) plastically, by ascending bubbles. The dominant failure mechanism is the one requiring the least gas overpressure (e.g., Z. Sun & Santamarina, 2019), which we compute from Equations 2, 7, and 8. This dominant overpressure and the corresponding mechanism is shown in Figures 11a and 11b for two clay consolidation states, $OCR = 0.5$ (a; representing short settling time of $t_s = 3$ weeks) and $OCR = 1$ (b; $t_s = 6$ weeks). These low OCR values are representative of the loose state of our system, which compacted under its own weight only. As expected, the failure pressure mostly increases with increasing clay thickness h_c. For loosely compacted clays (Figure 11a), the mode of preferred failure transitions from dome to bubble at $h_c \simeq 1$ cm. For stiffer, more consolidated layers (Figure 11b), the mode of failure transitions from doming to brittle faulting at $h_c \simeq 0.7$ cm, and from faulting to bubbles (plastic) at $h_c \simeq 2$ cm.

A phase diagram showing the expected mode of failure as a function of OCR and clay thickness h_c is presented in Figure 11c. Values of $OCR > 1$ are of practical interest as in nature there are larger stresses that produce greater consolidation. Figure 11c shows that domes are predicted to be the preferred deformation mode for very thin layers (here $h_c < 1$ cm). For thicker layers, the mode of failure transitions with increasing h_c, first to brittle faulting creating a plug, and then to plastic: for soft clay ($OCR = 0.5$), layers thicker than 1 cm will degas by bubbles. In more rigid clays ($OCR = 1$) layers of intermediate thickness (here $1 \leq h_c \leq 2.25$ cm) will degas by lifting a faulted plug, while clays with $h_c > 2.25$ cm will still degas by bubbles. As the clay compacts more (larger OCR), the transition from brittle to plastic occurs at increasingly larger h_c.

5. Discussion

5.1. Theory of Seal Deformation Applied to Experimental Results

Our experiments show that the mode of deformation controls the eventual PM type: Domes lead to Type-2 PM while brittle and plastic deformation create a Type-1 PM; for example, see Figures 6 and 8. Our analysis (Figure 11c) suggests that the mode of deformation and thus the eventual PM type co-depend on two experimental parameters: clay thickness h_c and settling time t_s. The time t_s controls the degree of consolidation (as measured by the OCR), thus affecting the clay elastic modulus (Equation S2 in Supporting Information S1) and shear strength c_u (Equation 5). t_s also affects the tensile strength, T_0 (Equation 2). Seal thickness h_c also affects all modes of

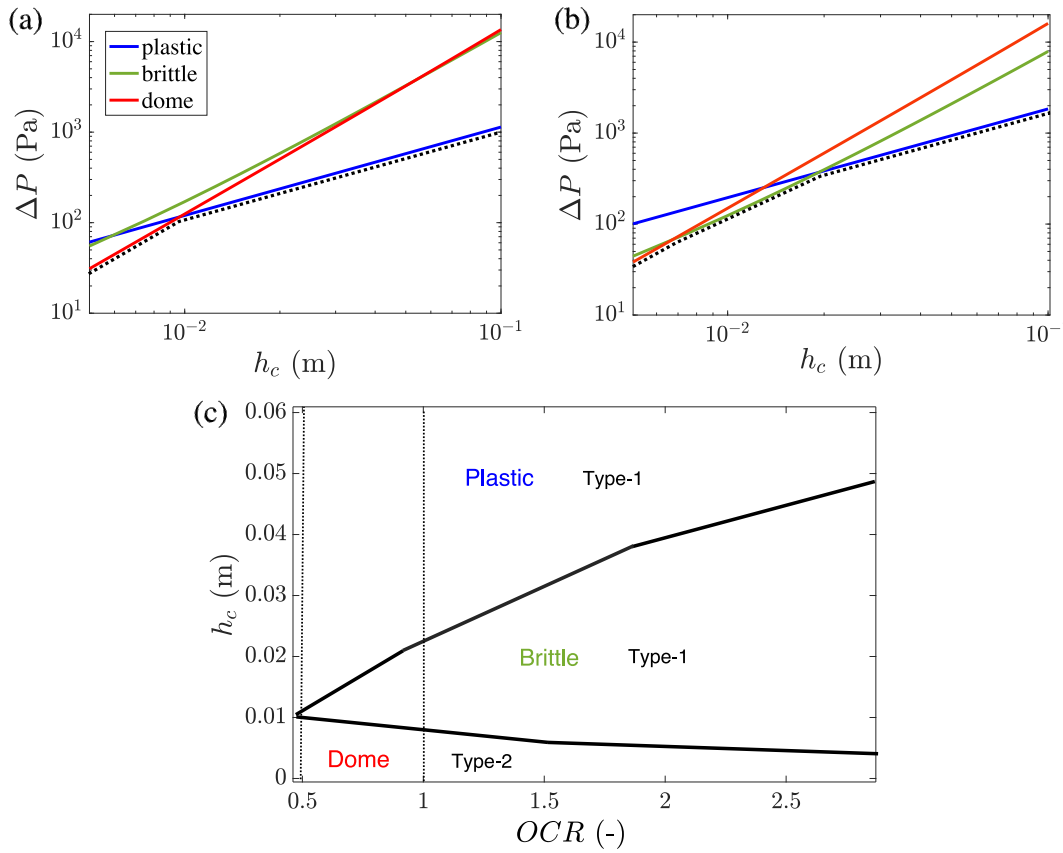

Figure 11. Calculated gas overpressure required to activate each of the 3 failure modes of the seal in our experiments (solid lines; Equation 2 in red, Equation 7 in green, and Equation 8 in blue), and expected PM types, as function of clay layer thickness h_c, for two different representative consolidation degrees: (a) $OCR = 0.5$; and (b) $OCR = 1$. The dominant deformation mode is set by the mechanism requiring the minimal value of ΔP (dotted black lines). (c) Theoretical phase diagram for the preferred (minimal ΔP) deformation mode, as function of clay layer thickness and OCR value, adding more OCR values in addition to those shown in (a, b).

failure, appearing directly or indirectly in all failure conditions (Equations 2, 3 and 8). In this way both h_c and t_s affect the strength for dome breach, and brittle and plastic failure. The theoretical phase diagram (Figure 11c) is in general in good agreement with the experimental data (phase diagram in Figure 8). Both the experiments and the theory suggest that doming would dominate for the thinnest layers, plastic deformation by bubble ascent for the thickest layers, and brittle faulting more dominant for intermediate layer thickness, with faulting in stiffer, more settled layers. A corresponding transition from Type-2 to Type-1 PM is seen experimentally and predicted theoretically. The experiments also support the theoretical prediction that the critical clay thickness (h_c) value at the transition between Type-2 to Type-1 PM increases with the system size (width of the experimental cell); for example, in Figure 8 experiment #5E (wider cell) is deformed by doming whereas #1C (narrower cell, nearly identical h_c) produces faulting.

Despite the overall agreement between our experimental data and theory, the theoretical critical pressure in Figures 11a and 11b cannot be directly validated by our experiments. This is because once the gas pocket detaches from the inlet (syringe) and ascends (see e.g. Movie S1), its pressure is no longer associated with that of the reservoir (inlet, where we measure the pressure, cf. Figure S1 in Supporting Information S1). Instead, we could estimate bounds: the inlet pressure provides an upper bound, whereas $(\rho_w - \rho_g)gh_g$ provides a lower bound, where h_g is the height of the detached gas pocket. The theoretical values in Figures 11a and 11b, ~100–1,000 Pa, are well within the bounds evaluated from our experiments.

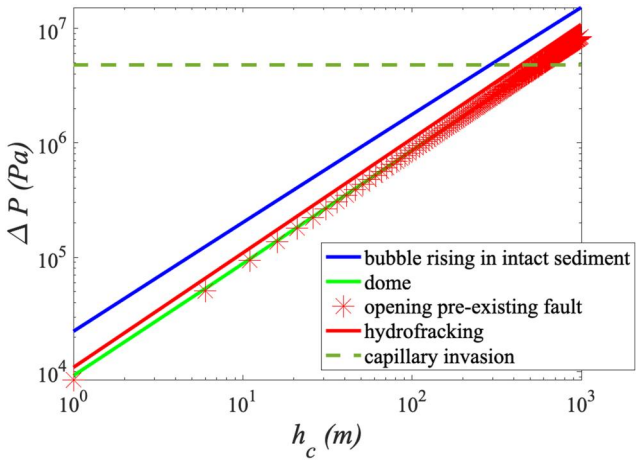

Figure 12. Calculated overpressure required to initiate deformation under field conditions. Doming (solid green line; Equation 12) and opening of existing faults and fractures (red stars; $\Delta P = \sigma'_v$) require nearly the same overpressure, and are the two favored deformation modes. Hydrofracking, that is, opening new fractures, requires only slightly higher overpressure (solid red line; Equation 4). Gas Bubbles rising freely in the sediment (blue line; Equation 8) are unlikely since they require much higher pressure than the brittle modes. Ignoring compaction, capillary invasion pressure is constant with depth (horizontal dashed line; Equation 13 with $r = 0.03$ μm). This phase diagram predicts that (until at least 1 km depth) gas overpressure will create domes and escape by bubbles opening pre-existing fractures, if such exist. Otherwise, domes will form, followed by hydrofracking and gas ascent in bubbles through them.

5.2. Theory of Seal Deformation Applied to Field Conditions

The application of the theoretically predicted deformation mechanisms to field conditions and scales requires (a) extending the calculations from 2D to 3D; (b) considering thicker seal layers, that is, h_c of 1–1,000 m (Koch et al., 2015; Moss & Cartwright, 2010); and (c) higher stresses. The expressions predicting the critical overpressure for the various deformation modes, provided below, are plotted versus clay thickness h_c in Figure 12.

Doming in 3D corresponds to an overpressure of Barry et al. (2012) and Koch et al. (2015),

$$\Delta P_{dome3D} = \frac{8}{3}\frac{E}{1-\nu}\frac{h_c w_{\max}}{a^4}\left(\frac{2h_c{}^2}{1+\nu} + w_{\max}{}^2\right) + \sigma'_v \quad (12)$$

where $w_{\max}$ is the dome maximum vertical deflection, and a is its lateral dimension. To compute the pressure in Equation 12 we use the parameter values for a/h_c, $w_{\max}/a$ and E from Koch et al. (2015), as discussed in Text S3 in Supporting Information S1. We note that this computation is poorly constrained by field observations due to the large uncertainty (wide bounds) in the values of the governing parameters a, $w_{\max}$ (Barry et al., 2012) and E (Koch et al., 2015). In addition, doming does not imply the mode of seal breaching, and therefore the above does not provide a critical overpressure for seepage.

Brittle deformation due to overpressure in field settings will either involve opening (Mode I failure) of pre-existing faults or fractures, or the creation of new faults (hydrofractures), through which gas will seep. "Plug-lifting" along faults, observed in some of our experiments, is not expected to occur in the field, as it is due to the small dimension of our experimental cell and our 2D settings. To lift a plug requires that the force exerted by the gas overpressure, exceeds the weight of the plug plus friction force on all four surfaces bounding the plug. Yet, these forces (stress times area) increase with system scale. Transmitting gas via an opening-mode pulse (i.e., rising penny-shaped bubbles (Boudreau et al., 2005)) only require stress to locally exceed a threshold. Thus, gas transmission through field-scale faults is expected to occur in rising disk-like bubbles, as observed in the gas-injection-into-gelatin experiments of Boudreau (2012) and Boudreau et al. (2005), and also in some of our thick-seal experiments, for example, Figure 5. To open a pre-exiting fracture the gas overpressure must exceed the effective confining stress, whereas to form and open a new hydrofracture requires an even higher overpressure (cf. Equation 4), see Figure 12.

A bubble can rise buoyantly in fractures once its buoyancy force exceeds the drag force, where the critical bubble size depends on its shape and size, and on layer thickness (Section 4.3.3). Extending our computations relying on the assumption of a spherical bubble (Equation 11) is beyond the scope of this paper.

Note that once one gas bubble ascends through a fault or fracture it decompacts the sediment in its pathway, locally reducing its strength (Equation 5), which in turn favors future gas ascent within this route, localizing it into a gas pipe.

Plastic deformation by bubbles forming in intact sediment (without fracturing) in the field is expected to require the same overpressure as in the experiments (Equation 8), see Figure 12 (blue line).

Capillary invasion was not discussed in relation to our experiments, due to the prohibitively high capillary entry pressures in the fine clay we used as seal. The gas overpressure required to push it into water-filled pore throats of size r is

$$\Delta P_{\text{cap}} = \frac{2\gamma_{gw}}{r} \quad (13)$$

where $\gamma_{gw} = 0.072$ N/m is gas-water surface tension. The pore sizes in natural clays span a wide range which is hard to constrain. Here, for simplicity we assume a constant radius with depth, using a value of $r = 0.03$ μm, measured as the dominant pore size in unconfined shale (Makhnenko et al., 2017), providing an overpressure of $\Delta P_{cap} \sim 4.8$ MPa (horizontal dashed line in Figure 12). If r decreases with confinement (depth) ΔP_{cap} will grow.

The mode of sediment failure that will be preferred is the one requiring the least pressure. Our theoretical analysis (Figure 12) suggests that doming will constitute the initial stage of many PMs; this agrees with the common interpretation of field-observed domes (Barry et al., 2012; A. Judd & Hovland, 2009; Koch et al., 2015). However, deformation by doming in *early stages* does not imply that doming will continue to be the dominant mode of deformation during *further* seal breaching and gas seepage. Following initial doming, our theoretical analysis (Figure 12) predicts gas escape by opening pre-existing faults and fractures (as seen experimentally, cf. Figure 5). Without pre-existing faults, hydro-fracturing is expected to occur, at slightly higher over-pressure. In domes, the overpressure required to fracture/fault the dome will be lowered relative to those required to fracture a flat seal, due to the extensional fiber stresses exerted by the dome flexure (for calculation of these stresses see Turcotte and Schubert (2014), Section 3.12), but we do not further pursue this calculation due to the very variable elastic modulus value.

Following conduit opening, gas bubbles will rise once reaching a critical radius, set by layer thickness and bubble geometry, leaving an elongated weakened pipe-like structure behind. We do not expect bubbles to rise freely in *undisturbed* sediment, due to the large pressure required, which is much higher than that to create a hydrofracture. Once bubbles (rising in either faults or fractures) reach the seal surface, they may create a PM via "erosive fluidization" (Cartwright & Santamarina, 2015): gas eruption ejects sediments to the shoulder of a PM, eroding the surface and creating a depression (e.g., Figures 5 and 4). This PM formation process constitutes a combination of several different mechanisms for gas transport to the surface that were discussed earlier. We emphasize that our experiments indicate that fluidization and associated erosion do not require a fluid jet (as suggested by Cartwright and Santamarina (2015)).

5.3. Implications From Table-Top Experiments and Theory to Natural Pockmarks

Linking between table-top laboratory experiments and field observations of pockmarks is challenging due to the different spatial and temporal scales. PM formation involves multiple scales in time—e.g. long quiescent periods of gas pressure buildup versus short periods in which gas seeps and pressure drops, and in space—e.g. PM depth, width, and dimensions of gas pipe and the disturbed zone around it. Furthermore, these are interrelated: the spatial scales evolve in time, such that for example, older pockmarks tend to be larger than younger ones (Andresen et al., 2021). In addition, in the field, PMs are often not isolated, but rather interact and depend on each other. Nonetheless, the mechanisms and trends observed in table-top experiments are qualitatively comparable to field observations.

Our experiments provide novel and unique data of the entire process of gas seepage from the reservoir to the surface (sea floor), that is, the initial pressure-induced seal failure followed by the passage of gas through the seal, and finally the formation of PMs at the surface, where gas seeps out (Figure 6). The deformation mechanisms forming the PMs differ between experimental and field conditions: In experiments either brittle failure or ascent of relatively spherical bubbles in liquefied clay can occur (depending on experimental setting), whereas in the field brittle deformation is expected to dominate, with elongated bubbles rising through fractures or faults. The observations in the field regarding the role of faulting are equivocal: while some (e.g., Crutchley et al. (2021)) suggest that gas preferentially rises through vertical fractures instead of through pre-existing faults, others show that pre-exiting faults control gas escape (Hustoft et al., 2009). The mechanisms of seal breaching and bubble ascent (Figure 3) control not only the manner by which the gas seeps out to the surface but also the sediment suspension in the water column, the episodic nature of the seepage, and the eventual PM shape (Figure 6).

5.3.1. Gas Migration Through the Sediment

Based on analysis of fluid escape pipes morphology and their geological context using seismic sections, Løseth et al. (2011) and Cartwright and Santamarina (2015) concluded that pipes play a critical role in providing leakage pathways for trapped hydrocarbons through overlying seals. Løseth et al. (2011) suggested hydro-fracturing of the seal as the main mechanism for breaching and pipe formation. In contrast, Cartwright and Santamarina (2015) excluded over-pressurized fluid related processes (such as hydraulic fracturing, erosional fluidization and

capillary invasions) as the dominant mechanism forming pipes; instead, Cartwright and Santamarina (2015) suggested localized collapse due to volume loss and syn-sedimentary flow localization as possible mechanisms for pipe growth, where initiation might be controlled by the above over-pressurized fluid related mechanism. Our experiments support a combination of the processes suggested by Cartwright and Santamarina (2015) and Løseth et al. (2011). In our experiments we observe that during the initial stage escape features (bubbles, faults, domes) form by high pore pressure. After the initial weakened zone forms, pipes develop as disrupted zones by repeated material degradation (Figures 3 and 4). Pipes direct gas seepage from the reservoir, through the seal to the seafloor (Figure 4), in agreement with field data in Løseth et al. (2011) showing pipes traversing throughout the seal all the way to the seafloor. Our experimental observations also agree with the model suggested by Løseth et al. (2011): overpressure buildup and release via pipes, and the formation of a mound at the pipe upper terminus, resulting in ejection of fluidized sediment close to the surface (rather than from depth). Our experiments also agree with the common hypothesis (Cartwright and Santamarina (2015) and elsewhere) relating the termination of pipes at the seafloor to PMs.

Another finding in our experiments that is relevant to field conditions is our observation of a mixed seepage mechanism, in which bubble pulses rise along brittle fractures (Figure 5). Like the vertical gas pipes, the fractures or faults become liquefied pipes after bubbles traverse them, promoting transport of further bubble trains in these pipes. Our theoretical analysis indicates that this gas escape mode would be ubiquitous in nature, in agreement with Z. Sun and Santamarina (2019). This theoretical prediction is supported by field data in the form of micro-seismic events in soft sediments, attributed to bubble rise and escape via faults (Tary et al., 2012).

We note the ambiguity between the main PM components: It is difficult to identify in nature the exact location and geometry of the *active* gas pipe, as it located within a larger disturbed zone which also includes dormant pipes that have closed, leaving the sediment around them looser. This is obvious from for example, seismic reflections showing a disturbed zone (e.g., ∼100 m in R. Maia et al. (2016)) which is much wider than the active pipe. A wide disturbed zone, relict of older gas pathways, is also seen in our experiments (e.g., Figure 4). Further complexity arises from the interactions between the pipe and PM geometry evolution, namely the deepening of the PM on the expense of shortening of the pipe.

In terms of bubble geometry, our experiments show that the rising bubbles are flattened into disk shapes (Figure 5), similar to the reports in natural sediments by Marcon et al. (2021), and to the Boudreau et al. (2005) experiments of gas injection into gelatin. Furthermore, bubble disk radii were seen in our experiments to correlate with pipe widths, as seen in Figures 4d and 5 (Note that the final localized pipe width may be much narrower than the initially disturbed zone width, as shown in Figure 4d). Thus, pipe widths are expected to grow with bubble radii, which in turn increase with seal layer thickness (experimental observation showing increasing of bubble radius with clay thickness are presented in Figure S2 in Supporting Information S1). Hence, we expect the experimentally observed ∼cm-scale pipes to scale up to 10–100 m in natural sediments, as observed in the field (Cartwright & Santamarina, 2015; Crutchley et al., 2021). The elongated bubble shape implies that bubble rise can happen at lower bubble volumes than that predicted by Equation 11, as the drag force which resists the bubble migration is proportional to the cross-section in the direction of motion. As the confinement imposed by litho-static stress reduces with the bubble height within the sediment, near the sediment surface the bubbles may resume their spherical shapes (Z. Sun & Santamarina, 2019).

5.3.2. Pockmark Geometry

Our experimental observation of a transition from Type 2 to Type 1 PMs as seal thickness, h_c, increases, also correlates with deepening of PMs, that is, experimental Type 2 PMs are generally shallower (smaller PM depth, D) than Type 1 PMs. This agrees with trends observed in the field, where D also increases with h_c (e.g., Figure 10 of Brothers et al., 2012) and Type 2 PMs are often observed to be shallower than Type 1 PMs (Riboulot et al., 2016). We speculate that the transition between the PM types may arise from fracture spacing: layer thickness controls fracture spacing (Wu & Pollard, 1995), and thus thin layers will break into smaller blocks delineated by more closely spaced fractures, which in turn would favor creation of the complex, Type 2 PMs (e.g., experiment #1B in Figure 6). In contrast, large fracture spacing in thick layers would favor creation of simpler Type-1 p.m. with seepage from only a few, widely spaced fractures. Another feature we observed experimentally, which was also observed in the field, is that Type I PMs retain a relatively equidimensional depression shape (Figure 5), despite the rise of elongated bubbled, as seen by Crutchley et al. (2021); Hsu et al. (2021); Marcon

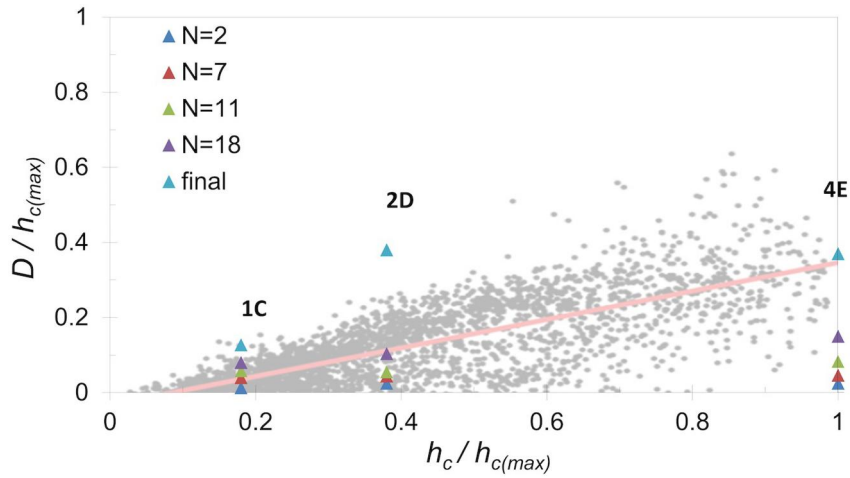

Figure 13. Comparing the pockmark depth D against clay thickness h_c between our experiments (triangles) and field observations (gray dots). To compare between the laboratory and field scale, we normalize both D and h_c by the maximal thickness $h_{c(\max)}$. The value of $h_{c(\max)}$ was 45 m for the field data, and 0.1 m for experiments (the value obtained in #4E). Also shown is the evolution of $D/h_{c(\max)}$ with number of seepage events N (legend) for the 3 presented experiments: #1C (brittle), # 2D and # 4E (both plastic deformation); see also Figure 7. Field data is from 3066 pockmarks offshore Maine, US (modified from Brothers et al. (2012); the pink line shows a linear trend for this population ($R^2 = 0.60$)).

et al. (2021). However, in cases where doming collapse led to clay breaching, seepage from multiple points between semi-rigid clay blocks resulted in Type-2 pockmarks with uneven depression (Figures 6 and 8).

Our observation of increasing pockmark depth D with time, until it traverses the entire clay layer (i.e., approaching the clay thickness h_c) (#2D in Figure 6), is in general agreement with field observations, for example, Andresen et al. (2021), which relates PM deepening to gas seepage events, as a consequence of sea level drops. In addition, Brothers et al. (2012) show varying pockmark depth related to the same hosting layer thickness (their Figure 10). A potential explanation is that the field data convolves different stages of PM development, since the depth (and thus D/h_c) changes with the number of events N (as we observed experimentally, cf. Figure 13). We also found a progressive increase in Type 1 PM width, L, by wall collapse (Figure 7b), in qualitative agreement with field observations of PM slopes steeper than the angle of repose, which suggest that these are active PMs, with *temporarily* non-stable slopes (Webb et al., 2009). The PM walls observed in our experiments are steeper than in the field (angle of $\sim 10^o$ (e.g., Andrews et al., 2010; Rogers et al., 2006; Schattner et al., 2016)). Furthermore, the increase in PM aspect ratio (depth vs. width; Figure 7c) differs from the relatively constant ratio observed in the field (Gontz, 2002), which is often used to deduce PM geometry from measurement of one of its dimensions (Brothers et al., 2012). These discrepancies could be due to reduced friction in the field following multiple seepage events and material degradation at long times in nature (vs. the short time of our experiments), as well as the artifact of additional frictional resistance (between the clay and the plexiglass walls) in our quasi-2D setup.

5.4. Temporal Evolution of Gas Escape

We observe episodic gas escape, with long quiescent periods interspersed by gas bubble ascent (either by deforming plastically the seal, or through fractures). Each seepage event is accompanied by an abrupt change in PM geometry, and weakening of the flow path (into a pipe). Similar episodic venting was seen in a north sea PM, from which gas flaring was observed in one expedition but not a few years later (Hustoft et al., 2009). Long quiescent period of over a decade with no PM geometry change was observed by Brothers et al. (2011), implying that it would be extremely hard to observe the short episodic venting during such periods. However, since previous work suggests that stress perturbations accelerate bubble escape from sediments (Katsman, 2019), it is not surprising that most observations of episodic gas emission from PMs, follow stress perturbations, for example, by earthquakes and storms (Christodoulou et al., 2023; Field & Jennings, 1987; Gontz et al., 2001; Hasiotis et al., 1996; Soter, 1999). Based on our experimental observations, we hypothesize that episodicity often characterizes gas seepage from PMs: each seepage event, which also deforms the PM, reflects something akin to a

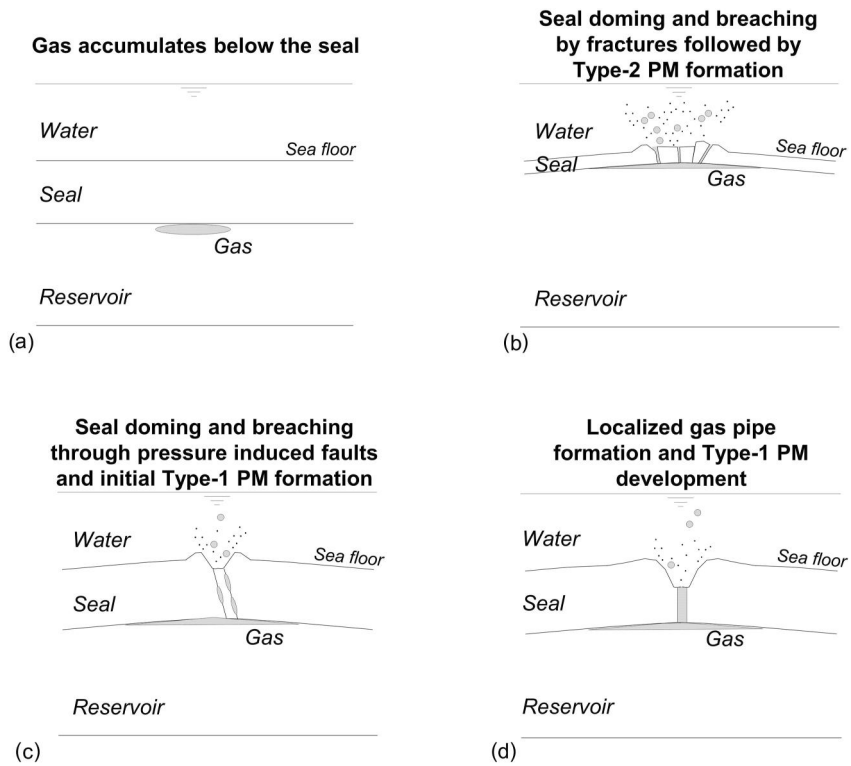

Figure 14. Schematic illustration summarizing the stages of pockmark formation expected in the field, based on theoretical insights from our experiments. (a) Gas accumulates at the top of the reservoir below the seal. Due to overpressure development the seal is deformed by doming, then gas seeps to the sea-floor thought the seal in one of the following seal breaching mechanisms: (b) Breaching of the seal by tensional fracturing. Then development of Type 2 pockmark; (c) pressure induced faults (as a consequence of brittle deformation of the seal). In this mechanism, sediment is eroded from the sea-floor and is suspended into the water by the seeping gas (sediment particles are presented as dots), progressively creating a morphological depression (Type 1 pockmark); (d) Eventually, after repeated material degradation (through the pressure induced faults presented in c), localized gas pipe through the seal is created.

magmatic eruption in a volcano: enough gas overpressure must be accumulated to overcome the overlying layer resistance to deformation and open a fracture, akin to dike opening by magma. Opening allows gas escape, which then drops the pressure until it again accumulates to cause another eruption. Finally, we note that magmatic eruptions and mud volcanoes can also occur in a continuous manner (Fallahi et al., 2017; Hidalgo et al., 2015; Kelemen & Aharonov, 1998), which, according to the above analogy, suggests a possibility of continuous gas seepage, which we did not observe in our experiments.

6. Conclusions

To understand submarine gas seeps and the associated surface deformation creating pockmarks, we developed an experimental model system composed of a reservoir (glass beads representing a sandy sediment) overlaid by a deformable seal (clay layer). We find that gas rises continuously through the reservoir and accumulates in a spatially limited zone at the base of the seal, due to the high capillary threshold of the fine-grained clay limiting gas invasion into it. Over time, sufficient gas overpressure accumulates to deform the clay and seep through it. Gas seepage was found to occur by either (a) doming of the seal and breaching of the dome by fracturing, resulting in disordered, Type-2, pockmarks; (b) brittle deformation that creates faults, through which the gas seeps; or (c) plastic deformation by gas bubbles ascending through the seal; both (b) and (c) form Type-1 (cone shaped) pockmarks, in thicker, more compliant layers. We also observe cases where gas seeps as elongated bubbles in faults, representing mixed deformation mode. The conditions where these deformation modes govern, especially in terms of layer thickness and consolidation of the layer (determining its stiffness), were computed theoretically. We find that seepage is often assisted by a positive feedback mechanism: pipe-like preferential conduits are

created by the rise of trains of bubbles, that liquefy and weaken these conduits. Faults can serve as the starting point for such pathways.

We use our table-top experiments to predict natural seepage and deformation by theoretically extrapolating our finding to field conditions. This analysis suggest that the initial stage of seal deformation by gas overpressure will create a dome (Figures 14a and 14b). Seepage is expected to happen by breaching of the dome by mode I fractures leading to Type-2 pockmark in thin clay layers, and by creation of hydrofractures or by flow through existing faults that eventually form Type-1 pockmark in thicker clay layers (Figure 14c). We hypothesize that as seen experimentally, episodic release of gas bubbles will form preferential conduits ("pipes") by locally weakening the clay in their passage, as well as progressively enlarging (in depth and width) a pockmark at the surface (Figure 14d).

In conclusion, our findings, which are in overall good agreement with field data, improve our understanding of natural pockmark formation. They also expose challenges in linking between laboratory and field observations, and the need for further field data at higher spatiotemporal resolution, complemented by more controlled laboratory tests.

Data Availability Statement

All data used to generate the figures and conclusions in the paper are available in Vaknin et al. (2024).

Acknowledgments
RH and EH acknowledge partial support from the Ring Family Foundation for Research in Atmospheric & Global Changes Studies; RH also acknowledges partial support from the Israeli Science Foundation (#ISF-867/13), the Israel Ministry of Agriculture and Rural Development (#821-0137-13), and from the Engineering and Physical Sciences Research Council (EP/V050613/1). OK acknowledges support from the Israeli Science Foundation (#ISF-954/15).

References

Abrams, M. A. (2005). Significance of hydrocarbon seepage relative to petroleum generation and entrapment. *Marine and Petroleum Geology*, *22*(4), 457–477. https://doi.org/10.1016/j.marpetgeo.2004.08.003

Andresen, K., Dahlin, A., Kjeldsen, K., Røy, H., Bennike, O., Nørgaard-Pedersen, N., & Seidenkrantz, M.-S. (2021). The longevity of pockmarks–a case study from a shallow water body in northern Denmark. *Marine Geology*, *434*, 106440. https://doi.org/10.1016/j.margeo.2021.106440

Andrews, B. D., Brothers, L. L., & Barnhardt, W. A. (2010). Automated feature extraction and spatial organization of seafloor pockmarks, Belfast Bay, Maine, USA. *Geomorphology*, *124*(1–2), 55–64. https://doi.org/10.1016/j.geomorph.2010.08.009

Archer, D., Buffett, B., & Brovkin, V. (2009). Ocean methane hydrates as a slow tipping point in the global carbon cycle. *Proceedings of the National Academy of Sciences of the United States of America*, *106*(49), 20596–20601. https://doi.org/10.1073/pnas.0800885105

Athanasopoulos, G. A. (1993). Effects of ageing and overconsolidation on the elastic stiffness of a remoulded clay. *Geotechnical & Geological Engineering*, *11*(1), 51–65. https://doi.org/10.1007/bf00452921

Atkinson, J. (2017). *The mechanics of soils and foundations*. CRC Press.

Atkinson, J., Charles, J., & Mhach, H. (1994). Undrained hydraulic fracture in cavity expansion tests. In *International conference on soil mechanics and foundation engineering* (pp. 1009–1012).

Barry, M. A., Boudreau, B. P., & Johnson, B. D. (2012). Gas domes in soft cohesive sediments. *Geology*, *40*(4), 379–382. https://doi.org/10.1130/G32686.1

Bayon, G., Loncke, L., Dupré, S., Caprais, J.-C., Ducassou, E., Duperron, S., et al. (2009). Multi-disciplinary investigation of fluid seepage on an unstable margin: The case of the central Nile deep sea fan. *Marine Geology*, *261*(1–4), 92–104. https://doi.org/10.1016/j.margeo.2008.10.008

Berndt, C. (2005). Focused fluid flow in passive continental margins. *Philosophical Transactions of the Royal Society A: Mathematical, Physical & Engineering Sciences*, *363*(1837), 2855–2871. https://doi.org/10.1098/rsta.2005.1666

Berndt, C., Bünz, S., & Mienert, J. (2003). Polygonal fault systems on the mid-Norwegian margin: A long-term source for fluid flow. *Geological Society, London, Special Publications*, *216*(1), 283–290. https://doi.org/10.1144/gsl.sp.2003.216.01.18

Bøe, R., Rise, L., & Ottesen, D. (1998). Elongate depressions on the southern slope of the Norwegian trench (Skagerrak): Morphology and evolution. *Marine Geology*, *146*(1–4), 191–203. https://doi.org/10.1016/s0025-3227(97)00133-3

Böttner, C., Berndt, C., Reinardy, B. T., Geersen, J., Karstens, J., Bull, J. M., et al. (2019). Pockmarks in the witch ground basin, central North Sea. *Geochemistry, Geophysics, Geosystems*, *20*(4), 1698–1719. https://doi.org/10.1029/2018GC008068

Boudreau, B. P. (2012). The physics of bubbles in surficial, soft, cohesive sediments. *Marine and Petroleum Geology*, *38*(1), 1–18. https://doi.org/10.1016/j.marpetgeo.2012.07.002

Boudreau, B. P., Algar, C., Johnson, B. D., Croudace, I., Reed, A., Furukawa, Y., et al. (2005). Bubble growth and rise in soft sediments. *Geology*, *33*(6), 517–520. https://doi.org/10.1130/g21259.1

Bower, A. F. (2009). *Applied mechanics of solids*. CRC press.

Brothers, L. L., Kelley, J. T., Belknap, D. F., Barnhardt, W. A., Andrews, B. D., Legere, C., & Clarke, J. E. H. (2012). Shallow stratigraphic control on pockmark distribution in north temperate estuaries. *Marine Geology*, *329*, 34–45. https://doi.org/10.1016/j.margeo.2012.09.006

Brothers, L. L., Kelley, J. T., Belknap, D. F., Barnhardt, W. A., Andrews, B. D., & Maynard, M. L. (2011). More than a century of bathymetric observations and present-day shallow sediment characterization in Belfast bay, Maine, USA: Implication for pockmark field longeviy. *Geo-Marine Letters*, *31*(4), 237–248. https://doi.org/10.1007/s00367-011-0228-0

Brown, K. M. (1990). The nature and hydrogeologic significance of mud diapirs and diatremes for accretionary systems. *Journal of Geophysical Research*, *95*(B6), 8969–8982. https://doi.org/10.1029/jb095ib06p08969

Camerlenghi, A., Cita, M., Vedova, B. D., Fusi, N., Mirabile, L., & Pellis, G. (1995). Geophysical evidence of mud diapirism on the Mediterranean ridge accretionary complex. *Marine Geophysical Researches*, *17*(2), 115–141. https://doi.org/10.1007/bf01203423

Cartwright, J., Huuse, M., & Aplin, A. (2007). Seal bypass systems. *AAPG Bulletin*, *91*(8), 1141–1166. https://doi.org/10.1306/04090705181

Cartwright, J., & Santamarina, C. (2015). Seismic characteristics of fluid escape pipes in sedimentary basins: Implications for pipe genesis. *Marine and Petroleum Geology*, *65*, 126–140. https://doi.org/10.1016/j.marpetgeo.2015.03.023

Cathles, L. M., Su, Z., & Chen, D. (2010). The physics of gas chimney and pockmark formation, with implications for assessment of seafloor hazards and gas sequestration. *Marine and Petroleum Geology*, *27*(1), 82–91. https://doi.org/10.1016/j.marpetgeo.2009.09.010

Chapman, D. M., & Godin, O. A. (2001). Dispersion of interface waves in sediments with power-law shear speed profiles. II. Experimental observations and seismo-acoustic inversions. *Journal of the Acoustical Society of America*, *110*(4), 1908–1916. https://doi.org/10.1121/1.1401739

Chapuis, R. P., & Aubertin, M. (2003). On the use of the kozeny Carman equation to predict the hydraulic conductivity of soils. *Canadian Geotechnical Journal*, *40*(3), 616–628. https://doi.org/10.1139/t03-013

Christodoulou, D., Papatheodorou, G., Geraga, M., Etiope, G., Giannopoulos, N., Kokkalas, S., et al. (2023). Geophysical and geochemical exploration of the pockmark field in the Gulf of Patras: New insights on formation, growth and activity. *Applied Sciences*, *13*(18), 10449. https://doi.org/10.3390/app131810449

Crutchley, G. J., Mountjoy, J. J., Hillman, J. I. T., Turco, F., Watson, S., Flemings, P. B., et al. (2021). Upward-doming zones of gas hydrate and free gas at the bases of gas chimneys, New Zealand's hikurangi margin. *Journal of Geophysical Research: Solid Earth*, *126*(9), e2020JB021489. https://doi.org/10.1029/2020JB021489

Davies, R. J., Mathias, S. A., Moss, J., Hustoft, S., & Newport, L. (2012). Hydraulic fractures: How far can they go? *Marine and Petroleum Geology*, *37*(1), 1–6. https://doi.org/10.1016/j.marpetgeo.2012.04.001

de Mahiques, M. M., Schattner, U., Lazar, M., Sumida, P. Y. G., & de Souza, L. A. P. (2017). An extensive pockmark field on the upper Atlantic margin of southeast Brazil: Spatial analysis and its relationship with salt diapirism. *Heliyon*, *3*(2), e00257. https://doi.org/10.1016/j.heliyon.2017.e00257

Dickens, G. R. (2003). Rethinking the global carbon cycle with a large, dynamic and microbially mediated gas hydrate capacitor. *Earth and Planetary Science Letters*, *213*(3–4), 169–183. https://doi.org/10.1016/s0012-821x(03)00325-x

Dillon, W. P., Danforth, W., Hutchinson, D., Drury, R., Taylor, M., & Booth, J. (1998). Evidence for faulting related to dissociation of gas hydrate and release of methane off the southeastern United States. *Geological Society, London, Special Publications*, *137*(1), 293–302. https://doi.org/10.1144/gsl.sp.1998.137.01.23

Dupré, S., Woodside, J., Klaucke, I., Mascle, J., & Foucher, J.-P. (2010). Widespread active seepage activity on the Nile deep sea fan (offshore Egypt) revealed by high-definition geophysical imagery. *Marine Geology*, *275*(1), 1–19. https://doi.org/10.1016/j.margeo.2010.04.003

Fallahi, M. J., Obermann, A., Lupi, M., Karyono, K., & Mazzini, A. (2017). The plumbing system feeding the lusi eruption revealed by ambient noise tomography. *Journal of Geophysical Research: Solid Earth*, *122*(10), 8200–8213. https://doi.org/10.1002/2017JB014592

Fauria, K. E., & Rempel, A. W. (2011). Gas invasion into water-saturated, unconsolidated porous media: Implications for gas hydrate reservoirs. *Earth and Planetary Science Letters*, *312*(1–2), 188–193. https://doi.org/10.1016/j.epsl.2011.09.042

Ferré, B., Jansson, P. G., Moser, M., Serov, P., Portnov, A., Graves, C. A., et al. (2020). Reduced methane seepage from arctic sediments during cold bottom-water conditions. *Nature Geoscience*, *13*(2), 144–148. https://doi.org/10.1038/s41561-019-0515-3

Field, M. E., & Jennings, A. E. (1987). Seafloor gas seeps triggered by a northern California earthquake. *Marine Geology*, *77*(1–2), 39–51. https://doi.org/10.1016/0025-3227(87)90082-x

Forwick, M., Baeten, N. J., & Vorren, T. O. (2009). Pockmarks in Spitsbergen fjords. *Norwegian Journal of Geology/Norsk Geologisk Forening*, *89*.

Franchi, F., Rovere, M., Gamberi, F., Rashed, H., Vaselli, O., & Tassi, F. (2017). Authigenic minerals from the Paola Ridge (southern Tyrrhenian Sea): Evidences of episodic methane seepage. *Marine and Petroleum Geology*, *86*, 228–247. https://doi.org/10.1016/j.marpetgeo.2017.05.031

García-Gil, S. (2003). A natural laboratory for shallow gas: The Rías Baixas (NW Spain). *Geo-Marine Letters*, *23*(3), 215–229. https://doi.org/10.1007/s00367-003-0159-5

Gay, A., Lopez, M., Cochonat, P., Séranne, M., Levaché, D., & Sermondadaz, G. (2006). Isolated seafloor pockmarks linked to BSRs, fluid chimneys, polygonal faults and stacked Oligocene-Miocene turbiditic palaeochannels in the Lower Congo Basin. *Marine Geology*, *226*(1–2), 25–40. https://doi.org/10.1016/j.margeo.2005.09.018

Goff, J. A. (2019). Modern and fossil pockmarks in the New England mud patch: Implications for submarine groundwater discharge on the middle shelf. *Geophysical Research Letters*, *46*(21), 12213–12220. https://doi.org/10.1029/2019GL084881

Gontz, A. M. (2002). Evolution of seabed pockmarks in Penobscot Bay, Maine (Electronic theses and dissertation, p. 598). The University of Maine. Retrieved from https://digitalcommons.library.umaine.edu/etd/598

Gontz, A. M., Belknap, D., Daniel, F., & Kelley, J. (2001). Evidence for changes in the Belfast bay pockmark field, Maine. In *Geological society of America, abstracts with programs* (Vol. 33).

Harrington, P. (1985). Formation of pockmarks by pore-water escape. *Geo-Marine Letters*, *5*(3), 193–197. https://doi.org/10.1007/bf02281638

Hasiotis, T., Papatheodorou, G., Kastanos, N., & Ferentinos, G. (1996). A pockmark field in the Patras Gulf (Greece) and its activation during the 14/7/93 seismic event. *Marine Geology*, *130*(3–4), 333–344. https://doi.org/10.1016/0025-3227(95)00131-x

Hidalgo, S., Battaglia, J., Arellano, S., Steele, A., Bernard, B., Bourquin, J., et al. (2015). SO2 degassing at Tungurahua volcano (Ecuador) between 2007 and 2013: Transition from continuous to episodic activity. *Journal of Volcanology and Geothermal Research*, *298*, 1–14. https://doi.org/10.1016/j.jvolgeores.2015.03.022

Holtzman, R., Szulczewski, M. L., & Juanes, R. (2012). Capillary fracturing in granular media. *Physical Review Letters*, *108*(26), 264504. https://doi.org/10.1103/physrevlett.108.264504

Hornbach, M. J., Saffer, D. M., & Holbrook, W. S. (2004). Critically pressured free-gas reservoirs below gas-hydrate provinces. *Nature*, *427*(6970), 142–144. https://doi.org/10.1038/nature02172

Hovland, M., Gardner, J., & Judd, A. (2002). The significance of pockmarks to understanding fluid flow processes and geohazards. *Geofluids*, *2*(2), 127–136. https://doi.org/10.1046/j.1468-8123.2002.00028.x

Hovland, M., Heggland, R., De Vries, M., & Tjelta, T. (2010). Unit-pockmarks and their potential significance for predicting fluid flow. *Marine and Petroleum Geology*, *27*(6), 1190–1199. https://doi.org/10.1016/j.marpetgeo.2010.02.005

Hovland, M., Judd, A. G., & Burke, R. (1993). The global flux of methane from shallow submarine sediments. *Chemosphere*, *26*(1), 559–578. https://doi.org/10.1016/0045-6535(93)90442-8

Hovland, M., & Sommerville, J. H. (1985). Characteristics of two natural gas seepages in the North Sea. *Marine and Petroleum Geology*, *2*(4), 319–326. https://doi.org/10.1016/0264-8172(85)90027-3

Hovland, M., Svensen, H., Forsberg, C. F., Johansen, H., Fichler, C., Fosså, J. H., et al. (2005). Complex pockmarks with carbonate-ridges off mid-Norway: Products of sediment degassing. *Marine Geology*, *218*(1–4), 191–206. https://doi.org/10.1016/j.margeo.2005.04.005

Hsu, C.-W., Marcon, Y., Römer, M., Pape, T., Klaucke, I., Loher, M., et al. (2021). Heterogeneous hydrocarbon seepage at mictlan asphalt knoll of the southern Gulf of Mexico. *Marine and Petroleum Geology*, *132*, 105185. https://doi.org/10.1016/j.marpetgeo.2021.105185

Hustoft, S., Bünz, S., Mienert, J., & Chand, S. (2009). Gas hydrate reservoir and active methane-venting province in sediments on <20 Ma young oceanic crust in the Fram Strait, offshore NW-Svalbard. *Earth and Planetary Science Letters*, *284*(1–2), 12–24. https://doi.org/10.1016/j.epsl.2009.03.038

Hustoft, S., Mienert, J., Bünz, S., & Nouzé, H. (2007). High-resolution 3d-seismic data indicate focussed fluid migration pathways above polygonal fault systems of the mid-Norwegian margin. *Marine Geology*, *245*(1–4), 89–106. https://doi.org/10.1016/j.margeo.2007.07.004

Ishihara, K. (1996). *Soil behavior in earthquake geotechnics*. Clarendon Press Oxford.

Jain, A. K., & Juanes, R. (2009). Preferential mode of gas invasion in sediments: Grain-scale mechanistic model of coupled multiphase fluid flow and sediment mechanics. *Journal of Geophysical Research: Solid Earth*, *114*(B8), B08101. https://doi.org/10.1029/2008jb006002

Jedari-Eyvazi, F., Bayrakci, G., Minshull, T. A., Bull, J. M., Henstock, T. J., Macdonald, C., & Robinson, A. H. (2023). Seismic characterization of a fluid escape structure in the North Sea: The Scanner Pockmark complex area. *Geophysical Journal International*, *234*(1), 597–619. https://doi.org/10.1093/gji/ggad078

Judd, A., & Hovland, M. (2009). *Seabed fluid flow: The impact on geology, biology and the marine environment*. Cambridge University Press.

Judd, A. G. (2003). The global importance and context of methane escape from the seabed. *Geo-Marine Letters*, *23*(3), 147–154. https://doi.org/10.1007/s00367-003-0136-z

Katsman, R. (2019). Methane bubble escape from gas horizon in muddy aquatic sediment under periodic wave loading. *Geophysical Research Letters*, *46*(12), 6507–6515. https://doi.org/10.1029/2019GL083100

Kelemen, P. B., & Aharonov, E. (1998). Periodic formation of magma fractures and generation of layered gabbros in the lower crust beneath oceanic spreading ridges. *Geophysical monograph*, *106*, 267–289.

King, L. H., & MacLean, B. (1970). Pockmarks on the scotian shelf. *Geological Society of America Bulletin*, *81*(10), 3141–3148. https://doi.org/10.1130/0016-7606(1970)81[3141:potss]2.0.co;2

Klaucke, I., Sarkar, S., Bialas, J., Berndt, C., Dannowski, A., Dumke, I., et al. (2018). Giant depressions on the Chatham rise offshore New Zealand–morphology, structure and possible relation to fluid expulsion and bottom currents. *Marine Geology*, *399*, 158–169. https://doi.org/10.1016/j.margeo.2018.02.011

Koch, S., Berndt, C., Bialas, J., Haeckel, M., Crutchley, G., Papenberg, C., et al. (2015). Gas-controlled seafloor doming. *Geology*, *43*(7), 571–574. https://doi.org/10.1130/g36596.1

Krämer, K., Holler, P., Herbst, G., Bratek, A., Ahmerkamp, S., Neumann, A., et al. (2017). Abrupt emergence of a large pockmark field in the German bight, southeastern North Sea. *Scientific Reports*, *7*(1), 1–8. https://doi.org/10.1038/s41598-017-05536-1

Lawal, M. A., Bialik, O. M., Lazar, M., Waldmann, N. D., Foubert, A., & Makovsky, Y. (2023). Modes of gas migration and seepage on the salt-rooted palmahim disturbance, southeastern Mediterranean. *Marine and Petroleum Geology*, *153*, 106256. https://doi.org/10.1016/j.marpetgeo.2023.106256

Linke, P., Pfannkuche, O., Torres, M., Collier, R., Witte, U., McManus, J., et al. (1999). Variability of benthic flux and discharge rates at vent sites determined by in situ instruments. *EOS transactions*, *80*, F509. (46 Fall Meet. Suppl).

Loncke, L., & Mascle, J. F. S. P. (2004). Mud volcanoes, gas chimneys, pockmarks and mounds in the Nile deep-sea fan (eastern Mediterranean): Geophysical evidences. *Marine and Petroleum Geology*, *21*(6), 669–689. https://doi.org/10.1016/s0264-8172(04)00036-4

Løseth, H., Wensaas, L., Arntsen, B., Hanken, N.-M., Basire, C., & Graue, K. (2011). 1000 m long gas blow-out pipes. *Marine and Petroleum Geology*, *28*(5), 1047–1060. https://doi.org/10.1016/j.marpetgeo.2010.10.001

Macelloni, L., Simonetti, A., Knapp, J. H., Knapp, C. C., Lutken, C. B., & Lapham, L. L. (2012). Multiple resolution seismic imaging of a shallow hydrocarbon plumbing system, Woolsey mound, northern Gulf of Mexico. *Marine and Petroleum Geology*, *38*(1), 128–142. https://doi.org/10.1016/j.marpetgeo.2012.06.010

Maia, R., Cartwright, J., & Andersen, E. (2016). Shallow plumbing systems inferred from spatial analysis of pockmark arrays. *Marine and Petroleum Geology*, *77*, 865–881. https://doi.org/10.1016/j.marpetgeo.2016.07.029

Makhnenko, R., Vilarrasa, V., Mylnikov, D., & Laloui, L. (2017). Hydromechanical aspects of co2 breakthrough into clay-rich caprock. In *13th international conference on greenhouse gas control technologies, GHGT-13, 14–18 November 2016, Lausanne, Switzerland*. In *Energy procedia* (Vol. 114, pp. 3219–3228). https://doi.org/10.1016/j.egypro.2017.03.1453

Marchi, M., Gottardi, G., & Soga, K. (2014). Fracturing pressure in clay. *Journal of Geotechnical and Geoenvironmental Engineering*, *140*(2), 04013008. https://doi.org/10.1061/(ASCE)GT.1943-5606.0001019

Marcon, Y., Kelley, D., Thornton, B., Manalang, D., & Bohrmann, G. (2021). Variability of natural methane bubble release at southern hydrate ridge. *Geochemistry, Geophysics, Geosystems*, *22*(10), e2021GC009894. https://doi.org/10.1029/2021GC009894

Marcuson, W. F., & Wahls, H. E. (1972). Time effects on dynamic shear modulus of clays. *Journal of the Soil Mechanics and Foundations Division*, *98*(12), 1359–1373. https://doi.org/10.1061/JSFEAQ.0001819

Mayne, P. W. (2001). Stress-strain-strength-flow parameters from enhanced in-situ tests. In *Proceedings of the international conference on in situ measurement of soil properties and case histories* (pp. 27–47). Bali.

Mazzini, A., Ivanov, M. K., Nermoen, A., Bahr, A., Bohrmann, G., Svensen, H., & Planke, S. (2008). Complex plumbing systems in the near subsurface: Geometries of authigenic carbonates from dolgovskoy mound (black sea) constrained by analogue experiments. *Marine and Petroleum Geology*, *25*(6), 457–472. https://doi.org/10.1016/j.marpetgeo.2007.10.002

McGinnis, D. F., Greinert, J., Artemov, Y., Beaubien, S. E., & Wüest, a. (2006). Fate of rising methane bubbles in stratified waters: How much methane reaches the atmosphere? *Journal of Geophysical Research*, *111*(C9), 1–15. https://doi.org/10.1029/2005JC003183

Morel-Seytoux, H. J. (1993). Capillary barrier at the interface of two layers. In D. Russo & G. Dagan (Eds.), *Water flow and solute transport in soils: Developments and applications* (pp. 136–151). Springer Berlin Heidelberg. https://doi.org/10.1007/978-3-642-77947-3_10

Moss, J., & Cartwright, J. (2010). The spatial and temporal distribution of pipe formation, offshore Namibia. *Marine and Petroleum Geology*, *27*(6), 1216–1234. https://doi.org/10.1016/j.marpetgeo.2009.12.013

Mukabi, J. N., & Hossain, Z. (2011). Characterization and modeling of various aspects of pre-failure deformation of clayey geomaterials–applications in modelling. In *Proceedings. 1st international conference on geotechnique, environment & construction materials, geomat, mie, Japan.*

Nermoen, A., Galland, O., Jettestuen, E., Fristad, K., Podladchikov, Y., Svensen, H., & Malthe-Sørenssen, A. (2010). Experimental and analytic modeling of piercement structures. *Journal of Geophysical Research*, *115*(B10). https://doi.org/10.1029/2010JB007583

Neuzil, C. E. (1994). How permeable are clays and shales? *Water Resources Research*, *30*(2), 145–150. https://doi.org/10.1029/93WR02930

Osborne, M. J., & Swarbrick, R. E. (1997). Mechanisms for Generating Overpressure in Sedimentary Basins: A Reevaluation1. *AAPG Bulletin*, *81*(6), 1023–1041. https://doi.org/10.1306/522B49C9-1727-11D7-8645000102C1865D

Ouyang, Z., & Mayne, P. W. (2018). Effective friction angle of clays and silts from piezocone penetration tests. *Canadian Geotechnical Journal*, *55*(9), 1230–1247. https://doi.org/10.1139/cgj-2017-0451

Perrin, H., Clavaud, C., Wyart, M., Metzger, B., & Forterre, Y. (2019). Interparticle friction leads to nonmonotonic flow curves and hysteresis in viscous suspensions. *Physical Review X*, *9*(3), 031027. https://doi.org/10.1103/PhysRevX.9.031027

Pilcher, R., & Argent, J. (2007). Mega-pockmarks and linear pockmark trains on the West African continental margin. *Marine Geology*, *244*(1), 15–32. https://doi.org/10.1016/j.margeo.2007.05.002

Plaza-Faverola, A., Bünz, S., & Mienert, J. (2011). Repeated fluid expulsion through sub-seabed chimneys offshore Norway in response to glacial cycles. *Earth and Planetary Science Letters*, *305*(3–4), 297–308. https://doi.org/10.1016/j.epsl.2011.03.001

Plaza-Faverola, A., Westbrook, G. K., Ker, S., Exley, R. J., Gailler, A., Minshull, T. A., & Broto, K. (2010). Evidence from three-dimensional seismic tomography for a substantial accumulation of gas hydrate in a fluid-escape chimney in the nyegga pockmark field, offshore norway. *Journal of Geophysical Research: Solid Earth*, *115*(B8). https://doi.org/10.1029/2009jb007078

Poryles, R., Vidal, V., & Varas, G. (2016). Bubbles trapped in a fluidized bed: Trajectories and contact area. *Physical Review E*, *93*(3), 032904. https://doi.org/10.1103/PhysRevE.93.032904

Ramos, G., Varas, G., Géminard, J.-C., & Vidal, V. (2015). Gas-induced fluidization of mobile liquid-saturated grains. *Physical Review E*, *92*(6), 062210. https://doi.org/10.1103/PhysRevE.92.062210

Räss, L., Simon, N. S., & Podladchikov, Y. Y. (2018). Spontaneous formation of fluid escape pipes from subsurface reservoirs. *Scientific Reports*, *8*(1), 11116. https://doi.org/10.1038/s41598-018-29485-5

Riboulot, V., Sultan, N., Imbert, P., & Ker, S. (2016). Initiation of gas-hydrate pockmark in deep-water Nigeria: Geo-mechanical analysis and modelling. *Earth and Planetary Science Letters*, *434*, 252–263. https://doi.org/10.1016/j.epsl.2015.11.047

Riedel, M., Villinger, H., Freudenthal, T., Pape, T., & Bohrmann, G. (2020). Thermal characterization of pockmarks across vestnesa and svyatogor ridges, offshore Svalbard. *Journal of Geophysical Research: Solid Earth*, *125*(12), e2020JB019468. https://doi.org/10.1029/2020JB019468

Rogers, J. N., Kelley, J. T., Belknap, D. F., Gontz, A., & Barnhardt, W. A. (2006). Shallow-water pockmark formation in temperate estuaries: A consideration of origins in the western gulf of Maine with special focus on Belfast bay. *Marine Geology*, *225*(1–4), 45–62. https://doi.org/10.1016/j.margeo.2005.07.011

Schattner, U., Lazar, M., Harari, D., & Waldmann, N. (2012). Active gas migration systems offshore northern Israel, first evidence from seafloor and subsurface data. *Continental Shelf Research*, *48*, 167–172. https://doi.org/10.1016/j.csr.2012.08.003

Schattner, U., Lazar, M., Souza, L., Ten Brink, U., & Mahiques, M. (2016). Pockmark asymmetry and seafloor currents in the Santos basin offshore Brazil. *Geo-Marine Letters*, *36*(6), 457–464. https://doi.org/10.1007/s00367-016-0468-0

Schneider von Deimling, J., Greinert, J., Chapman, N., Rabbel, W., & Linke, P. (2010). Acoustic imaging of natural gas seepage in the North Sea: Sensing bubbles controlled by variable currents. *Limnology and Oceanography: Methods*, *8*(5), 155–171. https://doi.org/10.4319/lom.2010.8.155

Schneider von Deimling, J., Hoffmann, J., Geersen, J., Koschinski, S., Lohrberg, A., Gilles, A., et al. (2023). Millions of seafloor pits, not pockmarks, induced by vertebrates in the North Sea. *Communications Earth & Environment*, *4*(1), 478. https://doi.org/10.1038/s43247-023-01102-y

Simonetti, A., Knapp, J. H., Sleeper, K., Lutken, C. B., Macelloni, L., & Knapp, C. C. (2013). Spatial distribution of gas hydrates from high-resolution seismic and core data, Woolsey mound, northern Gulf of Mexico. *Marine and Petroleum Geology*, *44*, 21–33. https://doi.org/10.1016/j.marpetgeo.2013.04.004

Skarke, A., Ruppel, C., Kodis, M., Brothers, D., & Lobecker, E. (2014). Widespread methane leakage from the sea floor on the northern US Atlantic margin. *Nature Geoscience*, *7*(9), 657–661. https://doi.org/10.1038/ngeo2232

Snieder, R., & Beukel, A. v. d. (2004). The liquefaction cycle and the role of drainage in liquefaction. *Granular Matter*, *6*(1), 1–9. https://doi.org/10.1007/s10035-003-0151-9

Soter, S. (1999). Macroscopic seismic anomalies and submarine pockmarks in the Corinth–Patras rift, Greece. *Tectonophysics*, *308*(1–2), 275–290. https://doi.org/10.1016/s0040-1951(99)00090-6

Sultan, N., Marsset, B., Ker, S., Marsset, T., Voisset, M., Vernant, a. M., et al. (2010). Hydrate dissolution as a potential mechanism for pockmark formation in the Niger delta. *Journal of Geophysical Research: Solid Earth*, *115*(B8), 1–33. https://doi.org/10.1029/2010JB007453

Sun, Q., Wu, S., Cartwright, J., & Dong, D. (2012). Shallow gas and focused fluid flow systems in the Pearl River mouth basin, northern South China Sea. *Marine Geology*, *315*, 1–14. https://doi.org/10.1016/j.margeo.2012.05.003

Sun, Z., & Santamarina, J. C. (2019). Grain-displacive gas migration in fine-grained sediments. *Journal of Geophysical Research: Solid Earth*, *124*(3), 2274–2285. https://doi.org/10.1029/2018JB016394

Svensen, H., Planke, S., Malthe-Sørenssen, A., Jamtveit, B., Myklebust, R., Eidem, T. R., & Rey, S. S. (2004). Release of methane from a volcanic basin as a mechanism for initial Eocene global warming. *Nature*, *429*(6991), 542–545. https://doi.org/10.1038/nature02566

Tary, J.-B., Geli, L., Guennou, C., Henry, P., Sultan, N., Çağatay, N., & Vidal, V. (2012). Microevents produced by gas migration and expulsion at the seabed: A study based on sea bottom recordings from the sea of Marmora. *Geophysical Journal International*, *190*(2), 993–1007. https://doi.org/10.1111/j.1365-246X.2012.05533.x

Turcotte, D., & Schubert, G. (2014). *Geodynamics* (3rd ed.). Cambridge University Press. https://doi.org/10.1017/CBO9780511843877

Ugural, A. (1999). *Stresses in plates and shells*. WCB/McGraw Hill.

Vaknin, I., Aharonov, E., Holtzman, R., & Katz, O. (2024). Data used to generate the figures and conclusions in the paper [Dataset]. *Figshare*. https://doi.org/10.6084/m9.figshare.24586926

Varas, G., Vidal, V., & Géminard, J.-C. (2009). Dynamics of crater formations in immersed granular materials. *Physical Review E*, *79*(2), 1–7. https://doi.org/10.1103/physreve.79.021301

Varas, G., Vidal, V., & Géminard, J.-C. (2011). Venting dynamics of an immersed granular layer. *Physical Review E*, *83*(1), 1–6. https://doi.org/10.1103/physreve.83.011302

Volfson, D., Tsimring, L. S., & Aranson, I. S. (2003). Partially fluidized shear granular flows: Continuum theory and molecular dynamics simulations. *Physical Review E*, *68*(2), 021301. https://doi.org/10.1103/PhysRevE.68.021301

Webb, K. E., Hemmer, O., Lepland, A., & Gray, J. S. (2009). Pockmarks in the inner Oslofjord, Norway. *Geo-Marine Letters*, *29*(2), 111–124. https://doi.org/10.1007/s00367-008-0127-1

Westbrook, G. K., Thatcher, K. E., Rohling, E. J., Piotrowski, A. M., Pälike, H., Osborne, A. H., et al. (2009). Escape of methane gas from the seabed along the West Spitsbergen continental margin. *Geophysical Research Letters*, *36*(15), L15608. https://doi.org/10.1029/2009gl039191

Wood, D. M. (1991). *Soil behavior and critical state soil mechanics*. Cambridge University Press. https://doi.org/10.1017/CBO9781139878272

Wu, H., & Pollard, D. D. (1995). An experimental study of the relationship between joint spacing and layer thickness. *Journal of Structural Geology*, *17*(6), 887–905. https://doi.org/10.1016/0191-8141(94)00099-l

Xu, C., Wang, X., Lu, X., Dai, F., & Jiao, S. (2018). Experimental study of residual strength and the index of shear strength characteristics of clay soil. *Engineering Geology*, *233*, 183–190. https://doi.org/10.1016/j.enggeo.2017.12.004